^{3}H and ^{3}He calculations without angular momentum decomposition

K. Topolnicki
Jagiellonian University, PL-30348 Kraków, Poland

(Received 17 October 2018; revised manuscript received 13 March 2019; published 30 April 2019)

Results for the three-nucleon (3N) bound state carried out using the three-dimensional (3D) formalism are presented. In this approach calculations are performed without the use of angular momentum decomposition and instead rely directly on the 3D degrees of freedom of the nucleons. In this paper, for the first time, 3D results for ^{3}He bound state with the inclusion of the screened Coulomb potential are compared to ^{3}H calculations. The ^{3}He calculations were made possible largely due to a new, faster implementation of the 3N force in 3D calculations. Additionally, using these results, matrix elements of simple current operators related to the description of β decay of the triton are given. All computations are carried out using the first generation of NNLO 2N and 3N forces from the Bochum-Bonn group.

DOI: 10.1103/PhysRevC.99.044004

I. INTRODUCTION

The three-dimensional (3D) approach is an alternative to traditional, partial wave decomposition based, few-nucleon calculations. The main characteristic of the new approach is that it does not rely on angular momentum decomposition and instead works directly with the (three-dimensional) momentum degrees of freedom of the nucleons. As a consequence, it is not necessary to numerically implement the heavily oscillating functions needed for partial wave calculations. This beneficial property opens up the possibility to perform calculations at higher energies and with longer-ranged potentials. The latter is explored in this paper for the ^{3}He bound state. Some introductory applications of the 3D approach were investigated by various research groups [1–3]. A very good, general introduction to the 3D approach is given in Ref. [4].

This paper is built on top of the work carried out in Refs. [3,5,6]. A previous paper [5] focused on 3D ^{3}H bound-state calculations with the inclusion of a three-nucleon (3N) force. Unfortunately the implementation of the 3N interaction used in Ref. [5] was very inefficient and required the numerical calculation of many-fold integrals each time a new 3N energy was tested for the existence of a bound state. In this paper a significant improvement to the implementation of the 3N force in 3D calculations is introduced. In practice this improvement allows a lot of the numerical work to be performed once and the results of this work can be reused many times when testing different energies for the existence of a bound state. After carrying out the initial computations and storing the results, calculations with a 3N force are not drastically more expensive than calculations with 2N forces only. With the new improved implementation of the 3N force, the 3D approach could make it possible to more freely test various 3N force models since 3D calculations do not require performing the partial decomposition procedure. This is especially important for ^{3}He bound-state calculations with a screened Coulomb force since a significant lowering of the amount of numerical work is required in order to perform calculations at many different values of the screening parameter.

Several additional improvements were made with respect to the previous work presented in Ref. [5]. An additional $\frac{3}{2}$ total isospin component is included in the calculations allowing for a much wider class of potentials to be used in 3D calculations. In this paper the first-generation NNLO nuclear interaction is used (as in Ref. [5]), however, the additional isospin component made it possible to include the screened Coulomb interaction for ^{3}He bound-state calculations and opened up the possibility to use more modern nuclear potentials in future computations. Furthermore, the results presented in this paper demonstrate that including potentials with a longer-range (screened Coulomb interaction) is possible within the 3D approach.

The paper is organized as follows. In Sec. II an introduction to the 3D bound-state calculations is provided. The Faddeev equation is introduced together with the operator form of the 3N bound and Faddeev states. This operator form allows states to be defined via sets of scalar functions of Jacobi momenta. These scalar functions are the main object of the 3D calculations and the Faddeev equation is transformed into a linear equation in a space spanned by the scalar functions. In Sec. III explicit expressions for the relevant linear operators, acting in the space spanned by the scalar functions, are given. Crucially Sec. III C contains details on the new, faster implementation of the 3N force in 3D calculations. Section IV contains information on the practical numerical realization of the calculations. This section also contains a presentation and discussion of the results of the calculations: the ^{3}H and ^{3}He bound state, and the matrix elements relevant to the triton β decay. Finally Sec. V contains the summary and outlook. Additionally, Appendix A contains a list of spin operators used in the operator form of the 3N bound and Faddeev states and Appendix B contains details related to the calculation of current operator matrix elements related to the triton β decay.

II. FORMALISM

Calculations of the 3N bound state are carried out within the Faddeev formalism. Results presented in this paper are obtained with a version of the Faddeev equation that was investigated in Ref. [5] and that does not use the 2N transition operator:

$$|\psi\rangle = \check{G}_0(E)(\check{V} + \check{V}^{(1)})(\check{1} + \check{P})|\psi\rangle. \quad (1)$$

In Eq. (1) $|\psi\rangle$ is a Faddeev component, $\check{G}_0(E)$ is the free propagator for energy E, $\check{V}$ is the two-nucleon potential between particles two and three, and $\check{V}^{(1)}$ is a part of the 3N force that is symmetric with respect to the exchange of particles two and three. Finally:

$$\check{P} = \check{P}_{12}\check{P}_{23} + \check{P}_{13}\check{P}_{23} \quad (2)$$

is composed from operators $\check{P}_{ij}$ that perform the exchange of two particles $i = 1\ldots3$, $j = 1\ldots3$ and the full 3N bound state wave function $|\Psi\rangle$ can be obtained from the Faddeev component $|\psi\rangle$ using:

$$|\Psi\rangle = (\check{1} + \check{P})|\psi\rangle. \quad (3)$$

The starting point of the calculations is an operator form of the 3N (Faddeev, bound) state from Refs. [5,6]. In this form a 3N state $|\phi\rangle$ can be written as:

$$\langle \boldsymbol{pq}; \left(t\,\frac{1}{2}\right) T M_T |\phi\rangle = \sum_{i=1}^{8} \phi_{tT}^{(i)}(p, q, \hat{\boldsymbol{p}}\cdot\hat{\boldsymbol{q}})\check{O}_i(\boldsymbol{p}, \boldsymbol{q})|\chi^m\rangle, \quad (4)$$

where $\boldsymbol{p}$, $\boldsymbol{q}$ are Jacobi momenta; t is the isospin in the two-nucleon subsystem; T is the total isospin; M_T is its projection ($-\frac{1}{2}$ for ^{3}H, $\frac{1}{2}$ for ^{3}He); the spin operators $\check{O}_{i=1\ldots8}(\boldsymbol{p}, \boldsymbol{q})$ are listed in Appendix A and $|\chi^{m=\pm\frac{1}{2}}\rangle = |(0\frac{1}{2})\frac{1}{2}m\rangle$ is a given spin state where the spins of the three nucleons are coupled to the total spin $\frac{1}{2}$ with projection m. The set of scalar functions $\phi_{tT}^{(i)}(p, q, \hat{\boldsymbol{p}}\cdot\hat{\boldsymbol{q}})$ in Eq. (4) for all indexes i, t, T fully determines the state $|\phi\rangle$. In further parts of the paper a notation will be used in which this whole set of scalar functions is referred to by the greek letter without the indexes and arguments. For example: the 3N states $|\phi\rangle$, $|\gamma\rangle$, $|\beta\rangle$, ... are defined by sets of scalar functions [from the operator form (4)] $\{\phi_{tT}^{(i)}(p, q, \hat{\boldsymbol{p}}\cdot\hat{\boldsymbol{q}})\}$, $\{\gamma_{tT}^{(i)}(p, q, \hat{\boldsymbol{p}}\cdot\hat{\boldsymbol{q}})\}$, $\{\beta_{tT}^{(i)}(p, q, \hat{\boldsymbol{p}}\cdot\hat{\boldsymbol{q}})\}$, ... and these sets will be simply referred to as $\phi, \gamma, \beta, \ldots$. Moreover, the scalar functions in $\phi, \gamma, \beta, \ldots$ span a linear space that will form the main stage of the 3D calculations and vectors from this space will also be referred to using the same greek letters $\phi, \gamma, \beta, \ldots$

The approach to solving (1) using the operator form (4) follows the procedure outlined in Refs. [3,5]. First the operator form of the Faddeev component (4) is plugged into the Faddeev equation (1). Next the spin dependencies are removed from the resulting equations as discussed in Sec. III. Finally the resulting expressions are transformed into the following equation:

$$\check{A}(E)\psi = \psi, \quad (5)$$

where $\check{A}(E)$ is an energy-dependent linear operator that acts in a space spanned by the scalar functions from (4) and ψ are scalar functions that define the Faddeev component. In practical calculations a slightly modified version of this equation:

$$\check{A}(E)\psi = \lambda\psi \quad (6)$$

is solved for various values of the energy E. Once a solution to (6) is found such that $\lambda = 1$ then ψ is also a solution to (5), E is the bound-state energy, and the solution to (1) can be reconstructed using (4) with the scalar functions ψ.

The operator $\check{A}$ from (5) can be split into several parts that correspond to the various operators that appear in the Faddeev equation (1). These parts correspond to the application of $\check{1} + \check{P}$ ($\check{A}_{1+P}$), $\check{G}_0(E)\check{V}$ ($\check{A}_{G_0V}$), $\check{G}_0(E)V^{\check{(1)}}$ ($\check{A}_{G_0V^{(1)}}$) onto the 3N state $|\psi\rangle$ (represented by the set of scalar functions ψ). In ^{3}He calculations, the two-nucleon force $\check{V}$ can be further split into the short nucleon-nucleon interaction $\check{V}_{\rm NN}$ and the longer-ranged screened Coulomb potential $\check{V}_{\rm C}(R)$:

$$\check{G}_0(E)\check{V} = \check{G}_0(E)\check{V}_{\rm NN} + \check{G}_0(E)\check{V}_{\rm C}(R), \quad (7)$$

where R is the screening radius. This results in the operator $\check{A}_{G_0V}$ being written as a sum of two parts that correspond to the short-range nuclear (NN) and long-range Coulomb (C) interaction:

$$\check{A}_{G_0V}(E) = \check{A}_{G_0V_{NN}}(E) + \check{A}_{G_0V_C}(E, R).$$

For ^{3}He, the effect of this separation is four linear operators (acting in the linear space spanned by the scalar functions) and an additional dependence on the screening radius R:

$$\begin{aligned}\check{A}(E) &= \check{A}(E, R)\\ &= \left[\check{A}_{\rm G_0V_{NN}}(E) + \check{A}_{\rm G_0V_C}(E, R) + \check{A}_{\rm G_0V^{(1)}}(E)\right]\check{A}_{\rm 1+P}. \end{aligned} \quad (8)$$

For the triton the $\check{A}$ is slightly less complicated and there are only three operators:

$$\check{A}(E) = \left[\check{A}_{\rm G_0V_{NN}}(E) + \check{A}_{\rm G_0V^{(1)}}(E)\right]\check{A}_{\rm 1+P}. \quad (9)$$

The explicit form of all these operators will be given in Sec. III.

In this paper Eq. (6) is solved with several significant improvements with respect to Ref. [5]. The first change is the addition of the screened Coulomb interaction for ^{3}He. Second, a third $t = 1, T = \frac{3}{2}$ isospin state is included in all calculations on top of $t = 0, T = \frac{1}{2}$ and $t = 1, T = \frac{1}{2}$, this change has the most significant impact on ^{3}He calculations that utilize proton-proton interactions. Third and most importantly, a new numerical integration scheme was developed to deal with the application of the 3N force in $\check{A}_{\rm G_0V^{(1)}}(E)$. The new scheme allows applications of $\check{A}_{\rm G_0V^{(1)}}(E)$ on scalar functions for a number of different energies to be carried out with very little numerical work compared to Ref. [5]. The new implementation of the 3N force significantly extends the possible applications of the 3D approach and the details on this new approach are given in Sec. III C. Finally, all results in this paper are obtained assuming charge dependence of the nucleon-nucleon interaction and using different proton-proton and neutron-proton versions of the 2N force (the neutron-neutron interaction is taken as the strong proton-proton potential).

III. EXPLICIT FORM OF OPERATORS ACTING ON SCALAR FUNCTIONS

This section contains details on the linear operators $\check{A}_{1+P}$, $\check{A}_{G_0V_{NN}}$, $\check{A}_{G_0V_C}$, and $\check{A}_{G_0V^{(1)}}$ from (8) and (9). These operators act in a space spanned by the scalar functions from the operator form (4) and are components of Eqs. (5) and (6). Equation (5) directly corresponds to the Faddeev equation (1) and the scalar functions obtained by solving (5) can be used to reconstruct the Faddeev components of the ^{3}H and ^{3}He bound state.

A. Permutation operator

The permutation operator $\check{1} + \check{P}$ is implemented in the 3D calculations as $\check{A}_{1+P}$. The approach used here is more general than the one used in Ref. [5] but also shares some similarities. Some additional details are available in Ref. [5] and in Chap. 10 of Ref. [7]. A sketch of the derivations is provided below.

First, the operator form from for the states $|\alpha\rangle$, $|\delta\rangle$ from (4) is inserted into both sides of:

$$|\delta\rangle = (\check{1} + \check{P})|\alpha\rangle. \tag{10}$$

Next the spin dependency is removed from this equation by projecting it from the left onto different spin states $\langle\chi^m|\check{O}_k(\boldsymbol{p}'\boldsymbol{q}')$ for $k = 1 \ldots 8$ and summing over m. This operation results in a set of coupled integral equations that involve the scalar functions α and δ that define $|\alpha\rangle$ and $|\delta\rangle$ via (4). Using basic algebraic transformations these coupled equations can be transformed into:

$$\delta = \check{A}_{1+P}\,\alpha, \tag{11}$$

where on the right-hand side $\check{A}_{1+P}$ is a linear operator acting in the space of scalar functions. Equation (11) defines the $\check{A}_{1+P}$ operator since α and δ are scalar functions that, together with (4), can be used to reproduce the states $|\alpha\rangle$ and $|\delta\rangle$ before and after the application of $\check{1} + \check{P}$.

The transformation of (10) into (11) and the implementation of $\check{A}_{1+P}$ requires the introduction of a number of additional functions. The explicit forms of all these functions are given below, but due to their significant complexity they are calculated using software for symbolic programming [8]. After their analytical forms are worked out, they are automatically translated into FORTRAN code.

Unlike Ref. [5] the action of the permutation on the combined isospin-spin state of the 3N system is considered. Instead of using the $F_{tt'T}$ coefficients from Ref. [5] the following functions are introduced:

$$F^{\mathrm{id}}_{t'T'k;tTi}(\boldsymbol{p}',\boldsymbol{q}') = \sum_m \left\langle \left(t'\tfrac{1}{2}\right)T' \right| \otimes \langle\chi^m|[\check{1}\otimes\check{O}_k(\boldsymbol{p}',\boldsymbol{q}')][\check{1}\otimes\check{O}_i(\boldsymbol{p}',\boldsymbol{q}')] \left| \left(t\tfrac{1}{2}\right)T \right\rangle \otimes |\chi^m\rangle, \tag{12}$$

$$F^{1223}_{t'T'k;tTi}(\boldsymbol{p}',\boldsymbol{q}') = \sum_m \left\langle \left(t'\tfrac{1}{2}\right)T' \right| \otimes \langle\chi^m|[\check{1}\otimes\check{O}_k(\boldsymbol{p}',\boldsymbol{q}')][\check{P}_{12}][\check{P}_{23}][\check{1}\otimes\check{O}_i(\boldsymbol{P}^{2312}(\boldsymbol{p}',\boldsymbol{q}'),\boldsymbol{Q}^{2312}(\boldsymbol{p}',\boldsymbol{q}'))] \left| \left(t\tfrac{1}{2}\right)T \right\rangle \otimes |\chi^m\rangle, \tag{13}$$

$$F^{1323}_{t'T'k;tTi}(\boldsymbol{p}',\boldsymbol{q}') = \sum_m \left\langle \left(t'\tfrac{1}{2}\right)T' \right| \otimes \langle\chi^m|[\check{1}\otimes\check{O}_k(\boldsymbol{p}',\boldsymbol{q}')][\check{P}_{13}][\check{P}_{23}][\check{1}\otimes\check{O}_i(\boldsymbol{P}^{2313}(\boldsymbol{p}',\boldsymbol{q}'),\boldsymbol{Q}^{2313}(\boldsymbol{p}',\boldsymbol{q}'))] \left| \left(t\tfrac{1}{2}\right)T \right\rangle \otimes |\chi^m\rangle, \tag{14}$$

where the tensor product $\otimes$ separates states and operators in the particle 1 subspace from the particle 2,3 subspace and $[\check{P}_{ij}]$ are the matrix representations of the operator exchanging particles i and j in the combined isospin-spin space of the 3N system. The functions $\boldsymbol{P}^{2313}$, $\boldsymbol{P}^{2312}$, $\boldsymbol{Q}^{2313}$, and $\boldsymbol{Q}^{2312}$ are a direct result of applying the permutation operator to Jacobi momentum eigenstates:

$$\begin{aligned}
\check{P}_{23}\check{P}_{12}|\boldsymbol{p}'\boldsymbol{q}'\rangle &= |\boldsymbol{P}^{2312}(\boldsymbol{p}',\boldsymbol{q}')\boldsymbol{Q}^{2312}(\boldsymbol{p}',\boldsymbol{q}')\rangle,\\
\boldsymbol{P}^{2312}(\boldsymbol{p}',\boldsymbol{q}') &= -\tfrac{1}{4}(2\boldsymbol{p}' + 3\boldsymbol{q}'),\\
\boldsymbol{Q}^{2312}(\boldsymbol{p}',\boldsymbol{q}') &= \boldsymbol{p}' - \tfrac{1}{2}\boldsymbol{q}',\\
\check{P}_{23}\check{P}_{13}|\boldsymbol{p}'\boldsymbol{q}'\rangle &= |\boldsymbol{P}^{2313}(\boldsymbol{p}',\boldsymbol{q}')\boldsymbol{Q}^{2313}(\boldsymbol{p}',\boldsymbol{q}')\rangle\\
\boldsymbol{P}^{2313}(\boldsymbol{p}',\boldsymbol{q}') &= -\tfrac{1}{4}(2\boldsymbol{p}' - 3\boldsymbol{q}')\\
\boldsymbol{Q}^{2313}(\boldsymbol{p}',\boldsymbol{q}') &= -\boldsymbol{p}' - \tfrac{1}{2}\boldsymbol{q}'.
\end{aligned}$$

The three parts of the permutation operator $\check{1} + \check{P} = \check{1} + \check{P}_{12}\check{P}_{23} + \check{P}_{13}\check{P}_{23}$ in Eq. (11) will be considered separately. If the first part of $\check{P} = \check{P}_{12}\check{P}_{23} + \check{P}_{13}\check{P}_{23}$, namely $\check{P}_{12}\check{P}_{23}$, is applied to a 3N state $|\alpha\rangle$ written in the form of Eq. (4) ($|\alpha\rangle$ is defined by a set of scalar functions α) then this results in a new 3N state $|\gamma\rangle$ that can also be written in the form from Eq. (4) ($|\gamma\rangle$ is defined by a set of scalar functions γ). This introduces the operator $\check{P}^{\mathrm{scalar}}_{1223}$ that is defined via the relation:

$$\left(\check{P}^{\mathrm{scalar}}_{1223}\alpha\right)^{(k)}_{t'T'}(|\boldsymbol{p}'|,|\boldsymbol{q}'|,\hat{\boldsymbol{p}}'\cdot\hat{\boldsymbol{q}}') = \gamma^{(k)}_{t'T'}(|\boldsymbol{p}'|,|\boldsymbol{q}'|,\hat{\boldsymbol{p}}'\cdot\hat{\boldsymbol{q}}') \tag{15}$$

or, after removing the spin dependencies and using basic algebraic operations on the resulting equations:

$$\begin{aligned}
&\gamma^{(k)}_{t'T'}(|\boldsymbol{p}'|,|\boldsymbol{q}'|,\hat{\boldsymbol{p}}'\cdot\hat{\boldsymbol{q}}')\\
&\quad= \sum_{tT}\sum_{i=1}^{8}\phi^{(i)}_{tT}(|\boldsymbol{P}^{2312}(\boldsymbol{p}',\boldsymbol{q}')|,|\boldsymbol{Q}^{2312}(\boldsymbol{p}',\boldsymbol{q}')|,\\
&\hat{\boldsymbol{P}}^{2312}(\boldsymbol{p}',\boldsymbol{q}')\cdot\hat{\boldsymbol{Q}}^{2312}(\boldsymbol{p}',\boldsymbol{q}'))C^{1223}_{t'T'k;tTi}(\boldsymbol{p}',\boldsymbol{q}'),
\end{aligned} \tag{16}$$

where the functions $C^{1223}_{t'T'k;tTi}$ are

$$C^{1223}_{t'T'k;tTi}(\boldsymbol{p}',\boldsymbol{q}') = \sum_{t''T''j} (F^{\mathrm{id}})^{-1}_{t'T'k;t''T''j}(\boldsymbol{p}',\boldsymbol{q}') F^{1223}_{t''T''j;tTi}(\boldsymbol{p}',\boldsymbol{q}') \tag{17}$$

and the inverse functions $(F^{\mathrm{id}})^{-1}_{t'T'k;t''T''j}$ are defined by the relation:

$$\sum_{t''T''j} (F^{\mathrm{id}})^{-1}_{t'T'k;t''T''j}(\boldsymbol{p}',\boldsymbol{q}') F^{\mathrm{id}}_{t''T''j;tTi}(\boldsymbol{p}',\boldsymbol{q}') = \delta_{t't}\delta_{T'T}\delta_{ki}. \tag{18}$$

The second part of the permutation operator $\check{P}_{13}\check{P}_{23}$ can be introduced in a completely analogous way by replacing everywhere in Eqs. (15)–(18) 12 by 13:

$$\left(\check{P}^{\mathrm{scalar}}_{1323}\alpha\right)^{(k)}_{t'T'}(|\boldsymbol{p}'|,|\boldsymbol{q}'|,\hat{\boldsymbol{p}}'\cdot\hat{\boldsymbol{q}}') = \gamma^{(k)}_{t'T'}(|\boldsymbol{p}'|,|\boldsymbol{q}'|,\hat{\boldsymbol{p}}'\cdot\hat{\boldsymbol{q}}'). \tag{19}$$

Or more precisely:

$$\begin{aligned}
&\gamma^{(k)}_{t'T'}(|\boldsymbol{p}'|,|\boldsymbol{q}'|,\hat{\boldsymbol{p}}'\cdot\hat{\boldsymbol{q}}') \\
&\quad = \sum_{tT}\sum_{i=1}^{8} \phi^{(i)}_{tT}(|\boldsymbol{P}^{2313}(\boldsymbol{p}',\boldsymbol{q}')|, |\boldsymbol{Q}^{2313}(\boldsymbol{p}',\boldsymbol{q}')|, \\
&\hat{\boldsymbol{P}}^{2313}(\boldsymbol{p}',\boldsymbol{q}')\cdot\hat{\boldsymbol{Q}}^{2313}(\boldsymbol{p}',\boldsymbol{q}'))C^{1323}_{t'T'k;tTi}(\boldsymbol{p}',\boldsymbol{q}').
\end{aligned} \tag{20}$$

Finally, the $\check{1}$ in $\check{1}+\check{P}$ is just the identity operator and does not change the scalar function. In the end:

$$\begin{aligned}
&(\check{A}_{1+\mathrm{P}}\,\alpha)^{(k)}_{t'T'}(|\boldsymbol{p}'|,|\boldsymbol{q}'|,\hat{\boldsymbol{p}}'\cdot\hat{\boldsymbol{q}}') \\
&\quad = \alpha^{(k)}_{t'T'}(|\boldsymbol{p}'|,|\boldsymbol{q}'|,\hat{\boldsymbol{p}}'\cdot\hat{\boldsymbol{q}}') + \left(\check{P}^{\mathrm{scalar}}_{1223}\alpha\right)^{(k)}_{t'T'}(|\boldsymbol{p}'|,|\boldsymbol{q}'|,\hat{\boldsymbol{p}}'\cdot\hat{\boldsymbol{q}}') \\
&\qquad + \left(\check{P}^{\mathrm{scalar}}_{1323}\alpha\right)^{(k)}_{t'T'}(|\boldsymbol{p}'|,|\boldsymbol{q}'|,\hat{\boldsymbol{p}}'\cdot\hat{\boldsymbol{q}}').
\end{aligned} \tag{21}$$

Additional details are available in Ref. [5] and in Chap. 10 of Ref. [7]. The numerical implementation of $\check{P}^{\mathrm{scalar}}_{1223}$ and $\check{P}^{\mathrm{scalar}}_{1323}$ requires the use of interpolations; the calculations presented in this paper use cubic Hermitian splines.

B. 2N potential

This section contains expressions necessary to implement the action of the 2N potential on the scalar functions from the operator form (4)—the $\check{A}_{G_0V}(E)$ operator in 3D calculations. Since the approach used in this section is similar to the methods presented in Ref. [5], below a simplified version of the derivations is presented. However, with the information given in this section it should be possible to recreate the numerical implementation.

It is well established (see, e.g., Ref. [9]) that the matrix element of the 2N force between 3N Jacobi momentum eigenstates $\langle \boldsymbol{p}'\boldsymbol{q}'|$, $|\boldsymbol{p}\boldsymbol{q}\rangle$ can be written as:

$$\begin{aligned}
&\langle \boldsymbol{p}'\boldsymbol{q}'|\check{V}|\boldsymbol{p}\boldsymbol{q}\rangle \\
&= \delta^3(\boldsymbol{q}'-\boldsymbol{q}) \sum_{i=1}^{6}\sum_{t'T'}\sum_{tT}\sum_{M_TM_{T'}} \delta_{tt'}\delta_{M_{T'}M_T} v_i^{t'T'tT}(p',p,\hat{\boldsymbol{p}}'\cdot\hat{\boldsymbol{p}}) \\
&\quad \times (\check{1}\otimes\check{w}_i(\boldsymbol{p}',\boldsymbol{p}))\left|\left(t'\tfrac{1}{2}\right)T'M_{T'}\right\rangle\left\langle\left(t\tfrac{1}{2}\right)TM_T\right|,
\end{aligned} \tag{22}$$

where $\check{1}\otimes\check{w}_i(p',p,\hat{\boldsymbol{p}}'\cdot\hat{\boldsymbol{p}})$ is a spin operator with $\check{w}_i(p',p,\hat{\boldsymbol{p}}'\cdot\hat{\boldsymbol{p}})$ acting in the space of particles 2 and 3. Any operator that can be written using (22) implicitly satisfies symmetries with respect to spatial rotations, parity inversion, time reversal, and particle exchange and is effectively defined by the set of scalar functions of the relative final and initial momenta $v_i^{t'T'tT}(p',p,\hat{\boldsymbol{p}}'\cdot\hat{\boldsymbol{p}})$. The spin operators $\check{w}_i(\boldsymbol{p}',\boldsymbol{p})$ from (22) are [9,10]

$$\begin{aligned}
\check{w}_1(\boldsymbol{p}',\boldsymbol{p}) &= \check{1} \\
\check{w}_2(\boldsymbol{p}',\boldsymbol{p}) &= \check{\boldsymbol{\sigma}}(1)\cdot\check{\boldsymbol{\sigma}}(2) \\
\check{w}_3(\boldsymbol{p}',\boldsymbol{p}) &= -i(\check{\boldsymbol{\sigma}}(1)+\check{\boldsymbol{\sigma}}(2))\cdot(\boldsymbol{p}'\times\boldsymbol{p}) \\
\check{w}_4(\boldsymbol{p}',\boldsymbol{p}) &= \check{\boldsymbol{\sigma}}(2)\cdot(\boldsymbol{p}'\times\boldsymbol{p})\check{\boldsymbol{\sigma}}(3)\cdot(\boldsymbol{p}'\times\boldsymbol{p}) \\
\check{w}_5(\boldsymbol{p}',\boldsymbol{p}) &= \check{\boldsymbol{\sigma}}(2)\cdot(\boldsymbol{p}'+\boldsymbol{p})\check{\boldsymbol{\sigma}}(3)\cdot(\boldsymbol{p}'+\boldsymbol{p}) \\
\check{w}_6(\boldsymbol{p}',\boldsymbol{p}) &= \check{\boldsymbol{\sigma}}(2)\cdot(\boldsymbol{p}'\times\boldsymbol{p})\check{\boldsymbol{\sigma}}(3)\cdot(\boldsymbol{p}'-\boldsymbol{p})
\end{aligned}$$

and are constructed from the relative momentum vector operators $\boldsymbol{p}'$, $\boldsymbol{p}$ and the spin vector operators $\check{\boldsymbol{\sigma}}(i)$ acting in the space of particles $i=1,2$.

In the previous paper [5] the operator form (22) was used to work out the numerical implementation of $\check{G}_0(E)\check{V}$ in three-dimensional bound-state calculations. This was achieved by inserting the operator form (4) of 3N states $|\alpha\rangle$, $|\gamma\rangle$, the 2N potential (22) and the momentum space expression for the free propagator:

$$\langle \boldsymbol{p}'\boldsymbol{q}'|\check{G}_0(E)|\boldsymbol{p}\boldsymbol{q}\rangle = \delta^3(\boldsymbol{p}-\boldsymbol{p}')\delta^3(\boldsymbol{q}-\boldsymbol{q}')\frac{1}{E-\frac{3}{4m}p^2-\frac{1}{2m}q^2} \tag{23}$$

into

$$\check{G}_0(E)\check{V}|\alpha\rangle = |\gamma\rangle,$$

and projecting the resulting equation onto a Jacobi momentum eigenstate $\langle \boldsymbol{p}'\boldsymbol{q}'|$. The spin dependency of the resulting equation was removed, using the same method as in Sec. III A, by projecting it from the left onto different spin states $\langle\chi^m|\check{O}_k(\boldsymbol{p}'\boldsymbol{q}')$ for $k=1\ldots8$ and summing over m. The result of these manipulations, after some algebraic transformations, is a linear relation:

$$\gamma = \check{A}_{G_0V}(E)\alpha, \tag{24}$$

which defines the energy E dependent operator $\check{A}_{G_0V}(E)$. It acts in the space of the set of scalar functions that define Faddeev component in Eq. (4). Applying the first part of the Faddeev equation (1), $\check{G}_0(E)\check{V}$, to a state $|\alpha\rangle$ written in the operator form (4) that is defined by a set of scalar functions α $[\alpha^{(k)}_{t'T'}(p',q',x'=\hat{\boldsymbol{p}}'\cdot\hat{\boldsymbol{q}}')]$ results in a new state $|\gamma\rangle$ that can be written in the same form (4) but with a different set of scalar functions γ $[\gamma^{(k)}_{t'T'}(p',q',x'=\hat{\boldsymbol{p}}'\cdot\hat{\boldsymbol{q}}')]$. The full form of

$\check{A}_{G_0V}(E)$ is

$$\begin{aligned}\gamma^{(k)}_{t'T'}(p',q',x') &= (\check{A}_{G_0V}(E)\alpha)^{(k)}_{t'T'}(p',q',x'=\hat{\boldsymbol{p}}'\cdot\hat{\boldsymbol{q}}')\\ &= \int d^3\boldsymbol{p}\sum_T\sum_{i=1}^{8}\sum_{j=1}^{6}\frac{1}{E-\frac{3}{4m}p'^2-\frac{1}{m}q'^2}v_j^{t'T't'T}(p',p,\hat{\boldsymbol{p}}'\cdot\hat{\boldsymbol{p}})\bar{L}_{kji}(\boldsymbol{p}',\boldsymbol{q}',\boldsymbol{p})\alpha^{(i)}_{t'T}(p,q',x)\\ &= \int_0^\infty dpp^2\int_{-1}^{1}dx\sum_T\sum_{i=1}^{8}\frac{1}{E-\frac{3}{4m}p'^2-\frac{1}{m}q'^2}\left\{\sum_{j=1}^{6}\int_0^{2\pi}d\phi\, v_j^{t'T't'T}(p',p,\hat{\boldsymbol{p}}'\cdot\hat{\boldsymbol{p}})\bar{L}_{kji}(\boldsymbol{p}',\boldsymbol{q}',\boldsymbol{p})\right\}\alpha^{(i)}_{t'T}(p,q',x),\end{aligned}\tag{25}$$

where the integral over the vector $\boldsymbol{p}$ is parametrized as:

$$\boldsymbol{p} = p(\sqrt{1-x^2}\cos\phi, \sqrt{1-x^2}\sin\phi, x)$$

with p being the magnitude of $\boldsymbol{p}$, ϕ being the azimuthal angle and x being the cosine of the polar angle. Additionally, using the scalar character of the equations, in Eq. (25):

$$\begin{aligned}\boldsymbol{p}' &= p'(\sqrt{1-x'^2},0,x'),\\ \boldsymbol{q}' &= q'(0,0,1)\end{aligned}$$

can be chosen. The $\bar{L}$ functions are defined as:

$$\bar{L}_{kji} \equiv \sum_l C^{-1}_{kl}L_{lji},$$

where the C^{-1}, L coefficients are defined in Eqs. (49), (30) from Ref. [5]. Due to their complexity these functions are calculated using software for symbolic programming [8] and automatically translated into FORTRAN code.

The curly brackets in Eq. (25) contain integrals

$$\begin{aligned}&I^{2N}_{t'T'T;k;i}(p',q',x',p,x)\\ &\quad=\sum_{j=1}^{6}\int_0^{2\pi}d\phi\, v_j^{t'T't'T}(p',p,\hat{\boldsymbol{p}}'\cdot\hat{\boldsymbol{p}})\bar{L}_{kji}(\boldsymbol{p}',\boldsymbol{q}',\boldsymbol{p})\end{aligned}\tag{26}$$

that can be performed once and reused later when applying $\check{G}_0(E)\check{V}$ to different states (which are defined by different scalar functions α) and using different energies.

Equation (25) can be used to perform numerical calculations with both the short-range and long-range 2N interactions. When calculating the bound state of ^{3}He with the screened Coulomb interaction, the operator $\check{A}_{G_0V}$ is further split into two parts:

$$\check{A}_{G_0V} = \check{A}_{G_0V_{NN}} + \check{A}_{G_0V_C}$$

that correspond to the short-range nuclear interaction and longer-ranged screened Coulomb force, respectively. The numerical implementation of both of these operators is very similar. The only practical difference is that in the longer-ranged part $\check{A}_{G_0V_C}$ the integrals $I^{2N}_{t'T'T;k;i}(p',q',x',p,x)$ from (26) are calculated using more integration points around $p'=p$ and $x'=x$. Examples of grid points in the p-x plane are shown in Fig. 1. Also the number of integration points along the azimuthal angle in Eq. (26) is increased, typically 256 Gaussian points were used compared to 16 or 64 points for the nuclear interaction.

For the results presented in this paper a screened Coulomb potential from Ref. [11] was used. The momentum space expressions for this interaction are given explicitly in Eqs. (A3) and (A4) in Ref. [11]. Solutions were obtained using the same, first generation, short-range NNLO 2N interaction as was used in Ref. [5] but use both the neutron-proton and proton-proton version of this interaction (the neutron-neutron interaction is approximated by the available proton-proton force).

C. 3N force

This section contains expressions necessary to implement the action of the 3N potential on the scalar functions from the operator form (4)—the $\check{A}_{G_0V^{(1)}}$ operator. The matrix element of the 3N force between 3N Jacobi momentum eigenstates

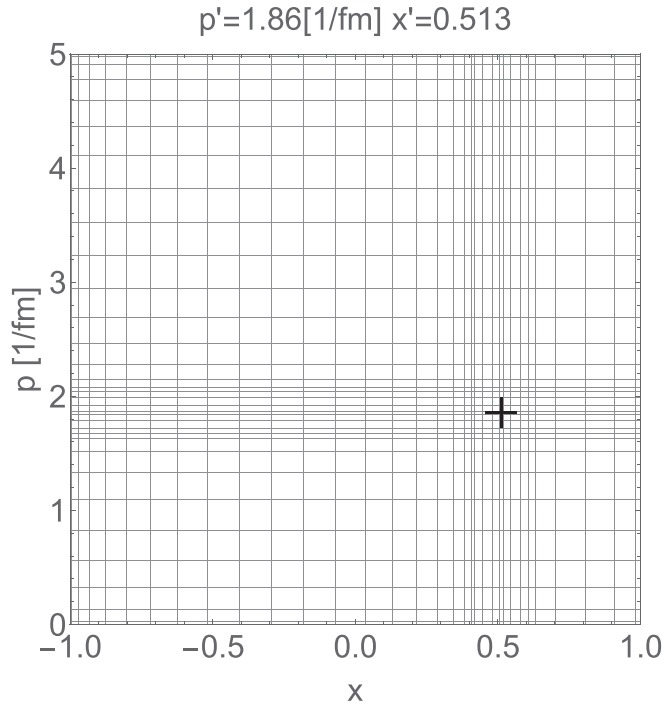

FIG. 1. Example integration points used for the screened Coulomb interaction in Eq. (25). Grid lines correspond to integration points in the x and p directions. The cross corresponds to (x', p'). Integration points in each direction are created by stitching together several sets of Gaussian quadrature points.

$\langle \boldsymbol{p}'\boldsymbol{q}'|$, $|\boldsymbol{p}\boldsymbol{q}\rangle$ can be written [5] as:

$$\langle \boldsymbol{p}'\boldsymbol{q}'|\check{V}^{(1)}|\boldsymbol{p}\boldsymbol{q}\rangle = \sum_{t'T'}\sum_{tT}\sum_{M_T M_{T'}} \delta_{TT'}\delta_{M_T M_{T'}} \check{V}^{(1)}_{tt'T}(\boldsymbol{p}', \boldsymbol{q}', \boldsymbol{p}, \boldsymbol{q}) \times \left|\left(t'\frac{1}{2}\right)T'M_{T'}\right\rangle\left\langle\left(t\frac{1}{2}\right)TM_T\right|, \tag{27}$$

where $\check{V}^{(1)}_{tt'T}(\boldsymbol{p}', \boldsymbol{q}', \boldsymbol{p}, \boldsymbol{q})$ is a spin operator acting in the space of three particles. The momentum dependence of this spin operator is limited by the requirement of spatial rotation invariance. Using this limitation the $\check{V}^{(1)}_{tt'T}(\boldsymbol{p}', \boldsymbol{q}', \boldsymbol{p}, \boldsymbol{q})$ can be written as a linear combination of 64 scalar functions and known spin operators (for more details see Appendix A in Ref. [12]). Unfortunately using this operator form does not directly impact numerical performance and for this reason the general operator form was not used and a new faster method of carrying out the necessary numerical integrations was developed instead. Using this new method was crucial in ^{3}He calculations with a 3N force since these calculations have to be repeated for various values of energy and the screening parameter. The results presented in this paper use the same first generation, NNLO 3N force as was used in Ref. [5].

In Ref. [5] the implementation of the second term of the Faddeev equation (1), $\check{G}_0(E)\check{V}^{(1)}$, in three-dimensional calculations was worked out. Similarly as in Sec. III B the implementation is an energy E dependent linear operator acting in the space of scalar functions that are used to define states in (4). This operator $\check{A}_{G_0V^{(1)}}(E)$ is defined via the relation:

$$\gamma = \check{A}_{G_0V^{(1)}}(E)\alpha, \tag{28}$$

where α $[\alpha^{(k)}_{t'T'}(p', q', x' = \hat{\boldsymbol{p}}' \cdot \hat{\boldsymbol{q}}')]$ are scalar functions that together with (4) can be used to reproduce the 3N state $|\alpha\rangle$ before the application of $\check{G}_0(E)\check{V}^{(1)}$ and γ $[\gamma^{(k)}_{t'T'}(p', q', x' = \hat{\boldsymbol{p}}' \cdot \hat{\boldsymbol{q}}')]$ are scalar functions that together with (4) can be used to reproduce the 3N state $|\gamma\rangle$ after the application of $\check{G}_0(E)\check{V}^{(1)}$. The full form of this relation is given explicitly in Ref. [5]:

$$\begin{aligned}
&[\check{A}^{3\mathrm{N}}(E)\alpha]^{(l)}_{t'T'}(p', q', \hat{\boldsymbol{p}}' \cdot \hat{\boldsymbol{q}}') \\
&\quad \equiv \gamma^{(l)}_{t'T'}(p', q', \hat{\boldsymbol{p}}' \cdot \hat{\boldsymbol{q}}') \\
&\quad = \int d^3\boldsymbol{p} d^3\boldsymbol{q} \frac{1}{E - \frac{3}{4m}p'^2 - \frac{1}{m}q'^2} \\
&\qquad \times \sum_t \sum_{i=1}^{8} \bar{E}^{t'tT'}_{li}(\boldsymbol{p}', \boldsymbol{q}', \boldsymbol{p}, \boldsymbol{q})\alpha^{(i)}_{tT'}(p, q, \hat{\boldsymbol{p}} \cdot \hat{\boldsymbol{q}}),
\end{aligned} \tag{29}$$

where the $\bar{E}^{t'tT'}_{li}$ functions are expressed in terms of the C^{-1} and E coefficients from Eqs. (49) and (27) in Ref. [5]:

$$\bar{E}^{t'tT'}_{ki} = \sum_l C^{-1}_{kl} E^{t'tT'}_{li}.$$

These functions, due to their complexity, are calculated using software for symbolic algebra [8] and automatically translated to FORTRAN code. Equation (29) is obtained by inserting the operator form of the Faddeev component (4), the 3N force (27) and the free propagator (23) into

$$|\gamma\rangle = \check{G}_0(E)\check{V}^{(1)}|\alpha\rangle$$

and, using the same methods as in Secs. III A and III B, removing the spin dependencies by projecting it from the left onto a Jacobi momentum eigenstate $\langle \boldsymbol{p}'\boldsymbol{q}'|$, different spin states $\langle\chi^m|\check{O}_k(\boldsymbol{p}'\boldsymbol{q}')$ for $k = 1 \ldots 8$ and summing over m.

It turns out that the parametrization of the sixfold integral in Eq. (29) is crucial to the numerical efficiency of the calculation. In Ref. [5] the following parametrization of the $\boldsymbol{p}$ and $\boldsymbol{q}$ vectors was used:

$$\begin{aligned}
\boldsymbol{p} &= p\big(\cos\phi_p\sqrt{1-x_p^2}, \sin\phi_p\sqrt{1-x_p^2}, x_p\big) \\
&= p\check{R}^{\phi_p}_{\hat{z}}\check{R}^{\theta_p}_{\hat{y}}(0, 0, 1)
\end{aligned} \tag{30}$$

$$\begin{aligned}
\boldsymbol{q} &= q\big(\cos\phi_q\sqrt{1-x_q^2}, \sin\phi_q\sqrt{1-x_q^2}, x_q\big) \\
&= q\check{R}^{\phi_q}_{\hat{z}}\check{R}^{\theta_q}_{\hat{y}}(0, 0, 1),
\end{aligned} \tag{31}$$

where $\check{R}^{\alpha}_{\hat{\boldsymbol{e}}}$ is a spatial rotation around the unit vector $\hat{\boldsymbol{e}}$ by angle α, p (q) is the magnitude of the momentum vector $\boldsymbol{p}$ ($\boldsymbol{q}$), ϕ_p (ϕ_q) is the azimuthal angle of vector $\boldsymbol{p}$ ($\boldsymbol{q}$) and x_p (x_q) is the cosine of the polar angle of vector $\boldsymbol{p}$ ($\boldsymbol{q}$). This parametrization results in the following form of Eq. (29):

$$\begin{aligned}
&\gamma^{(l)}_{t'T'}(p', q', \hat{\boldsymbol{p}}' \cdot \hat{\boldsymbol{q}}') \\
&\quad = \int_0^\infty dp\, p^2 \int_{-1}^{1} dx_p \int_0^{2\pi} d\phi_p \int_0^\infty dq\, q^2 \\
&\qquad \times \int_{-1}^{1} dx_q \int_0^{2\pi} d\phi_q \frac{1}{E - \frac{3}{4m}p'^2 - \frac{1}{m}q'^2} \\
&\qquad \times \sum_t \sum_{i=1}^{8} \bar{E}^{t'tT'}_{li}(\boldsymbol{p}', \boldsymbol{q}', \boldsymbol{p}, \boldsymbol{q})\alpha^{(i)}_{tT'}(p, q, \hat{\boldsymbol{p}} \cdot \hat{\boldsymbol{q}}),
\end{aligned}$$

where the angle argument of the scalar function $\alpha^{(i)}_{tT'}(p, q, \hat{\boldsymbol{p}} \cdot \hat{\boldsymbol{q}})$ has a complicated form:

$$\hat{\boldsymbol{p}} \cdot \hat{\boldsymbol{q}} = \big(\cos\phi_p \cos\phi_q + \cos(\phi_p - \phi_q)\sqrt{1-x_p^2}\sqrt{1-x_q^2}\big) \tag{32}$$

and the many-fold integral has to be calculated each time $\check{G}_0(E)\check{V}^{(1)}$ is applied. In the present work a different parametrization of the vector $\boldsymbol{q}$ is used:

$$\begin{aligned}
\boldsymbol{q} &= q\check{R}^{\phi_p}_{\hat{z}}\check{R}^{\theta_p}_{\hat{y}}\check{R}^{\phi_q}_{\hat{z}}\check{R}^{\theta_q}_{\hat{y}}(0, 0, 1) \\
&= \big(\sqrt{1-x_p^2}x_q\cos(\phi_p) \\
&\quad + \sqrt{1-x_q^2}(x_p\cos(\phi_p)\cos(\phi_q) - \sin(\phi_p)\sin(\phi_q)), \\
&\quad \sqrt{1-x_p^2}x_q\sin(\phi_p) + \sqrt{1-x_q^2}(x_p\sin(\phi_p)\cos(\phi_q) \\
&\quad + \cos(\phi_p)\sin(\phi_q)), \\
&\quad x_p x_q - \sqrt{1-x_p^2}\sqrt{1-x_q^2}\cos(\phi_q)\big).
\end{aligned} \tag{33}$$

The new parametrization (33) is related to the old parametrization (31) by a spatial rotation and the absolute value of the Jacobian determinant of the coordinate transformation from (30), (31) to (30), (33) is 1. Using (33) together with (30) leads to a very simple form of the third argument of the scalar

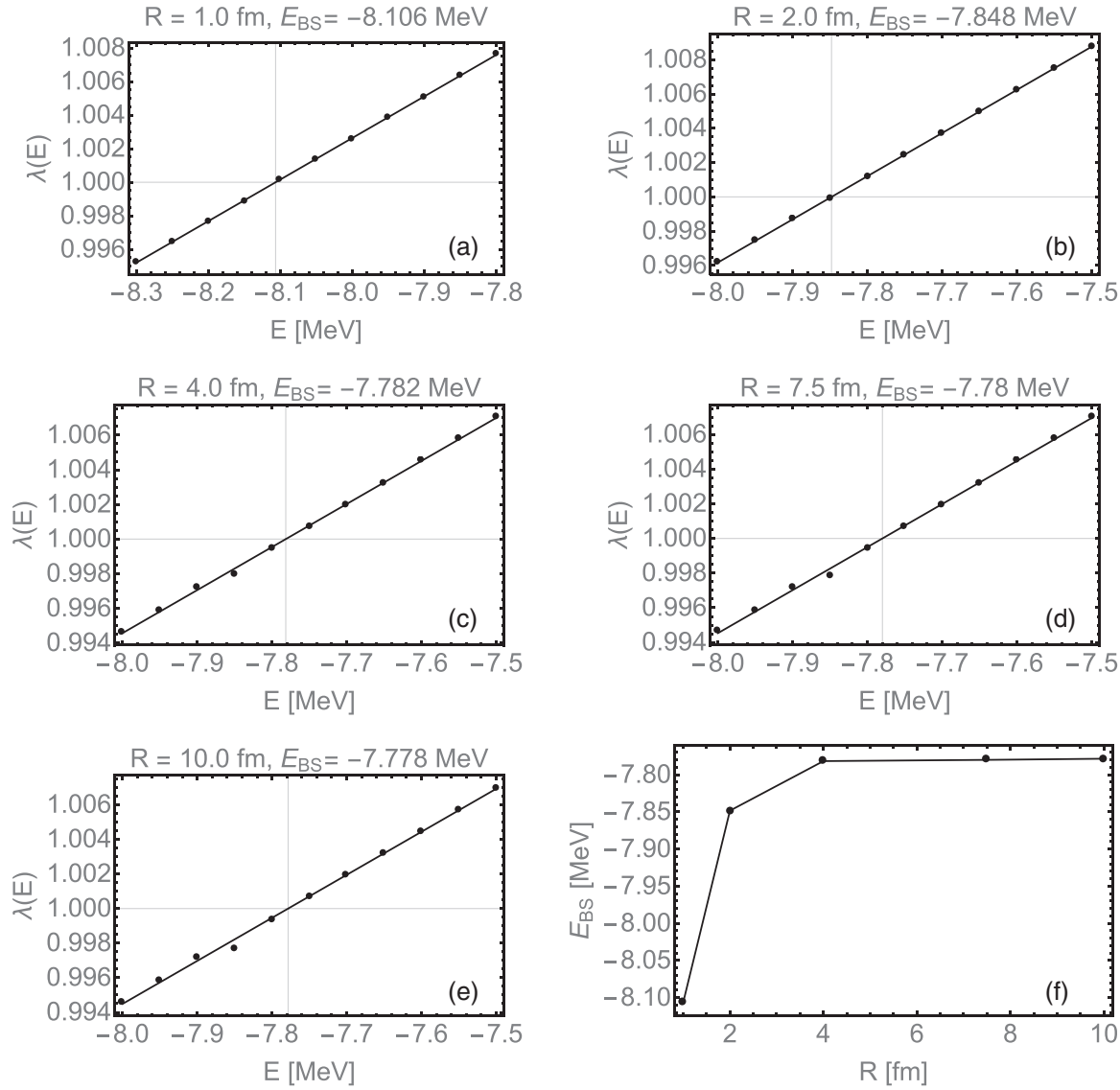

FIG. 2. (a)–(e): The eigenvalue λ that is closest to 1 as a functions of the energy E. The screened Coulomb potential from Ref. [11] was used and consecutive plots correspond to different screening radii used in Eq. (6). The crosses indicate the extrapolated bound state energies E_{BS} and $\lambda = 1$. (f): The extrapolated bound-state energy E_{BS} as a function of the screening radius R. Calculations were performed during the first run (see text) and use both the 2N and 3N force.

functions:

$$\hat{\boldsymbol{p}} \cdot \hat{\boldsymbol{q}} = x_{\boldsymbol{q}} = \cos\theta_{\boldsymbol{q}} \tag{34}$$

and allows Eq. (29) to be written as:

$$\begin{aligned}
&\gamma^{(l)}_{t'T'}(p', q', \hat{\boldsymbol{p}}' \cdot \hat{\boldsymbol{q}}' = x') \\
&= \int_0^\infty dp\, p^2 \int_0^\infty dq\, q^2 \int_{-1}^1 dx_{\boldsymbol{q}} \frac{1}{E - \frac{3}{4m}p'^2 - \frac{1}{m}q'^2} \sum_t \sum_{i=1}^8 \\
&\quad \times \left\{ \int_0^{2\pi} d\phi_{\boldsymbol{p}} \int_{-1}^1 dx_{\boldsymbol{p}} \int_0^{2\pi} d\phi_{\boldsymbol{q}} \bar{E}^{t't'T'}_{li}(\boldsymbol{p}', \boldsymbol{q}', \boldsymbol{p}, \boldsymbol{q}) \right\} \\
&\quad \times \alpha^{(i)}_{tT'}(p, q, \hat{\boldsymbol{p}} \cdot \hat{\boldsymbol{q}} = x_{\boldsymbol{q}}),
\end{aligned} \tag{35}$$

where the integrals in the curly brackets:

$$\begin{aligned}
&I^{3N}_{t;i}(p', q', x', p, q, x_{\boldsymbol{q}}) \\
&\quad = \int_0^{2\pi} d\phi_{\boldsymbol{p}} \int_{-1}^1 dx_{\boldsymbol{p}} \int_0^{2\pi} d\phi_{\boldsymbol{q}} \bar{E}^{t't'T'}_{li}(\boldsymbol{p}', \boldsymbol{q}', \boldsymbol{p}, \boldsymbol{q})
\end{aligned}$$

can be performed once, stored in arrays and reused. The possibility to reuse these integrals significantly reduces the numerical work needed to carry out the bound-state calculations, especially if the calculations are to be performed for a vast spectrum of bound-state energy candidates E. The downside of this approach is that that $I^{3N}_{t;i}(p', q', x', p, q, x_{\boldsymbol{q}})$ must be calculated and stored for a large number of parameters—the floating point parameters $p', q', x', p, q, x_{\boldsymbol{q}}$ and discrete indices t, i.

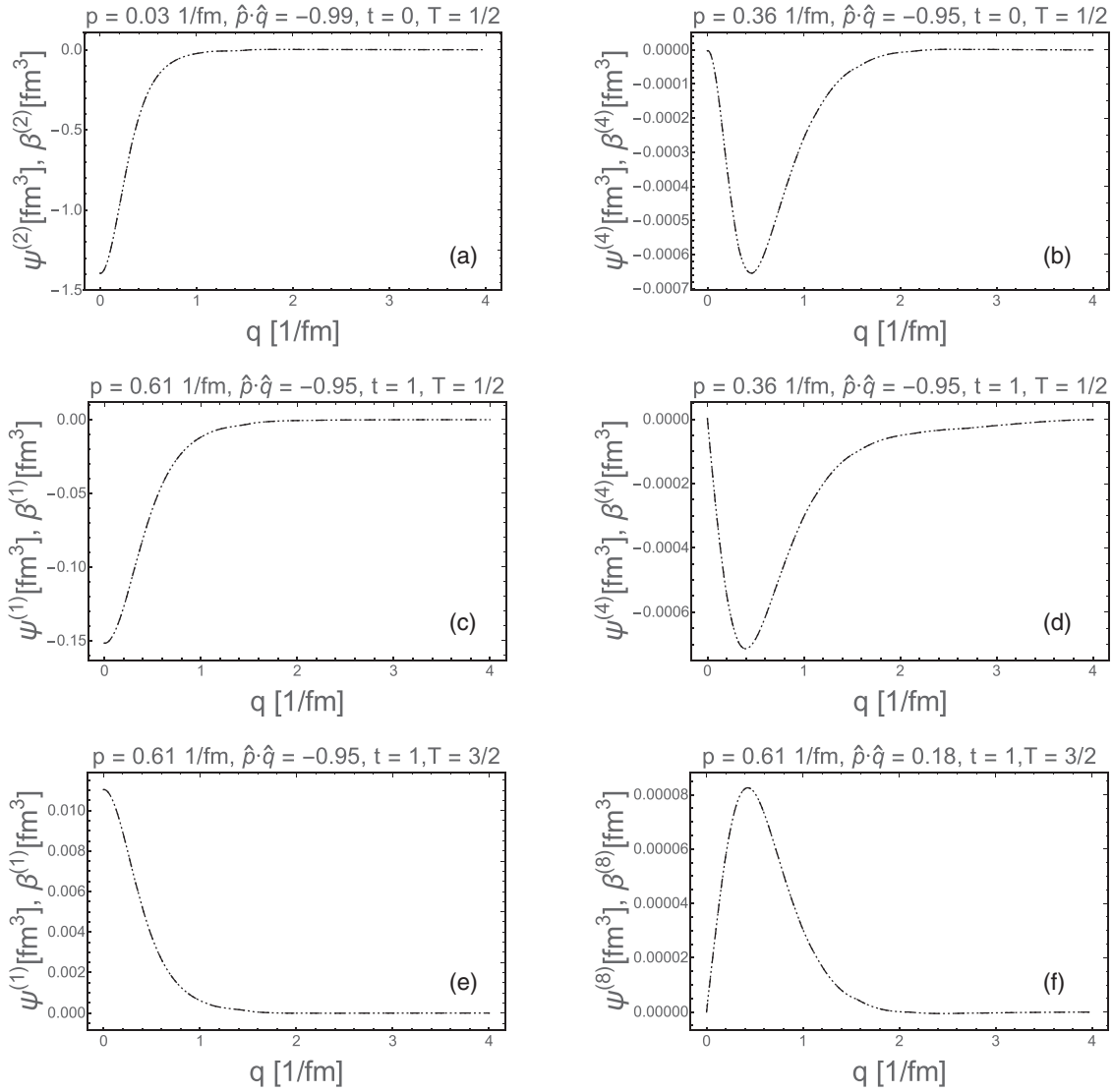

FIG. 3. Selected scalar functions for the Faddeev component of the ^{3}He bound state plotted as a function of the Jacobi momentum $\boldsymbol{q}$ magnitude. Scalar functions ψ obtained from the Arnoldi algorithm using (41) are marked using dashed lines while functions β obtained using (42) are marked using dotted lines. The correct solution to (5) implies that $\psi = \beta$ and since all lines essentially overlap this verifies the solution. Plots (a), (b) contain the $t = 0, T = \frac{1}{2}$ isospin component; (c), (d) contain the $t = 1, T = \frac{1}{2}$ isospin component; and (e), (f) contain the $t = 1, T = \frac{3}{2}$ isospin component. Calculations were performed during the second run (see text) with improved numerics and using both the 2N and 3N nuclear forces and a screened Coulomb interaction form [11] with screening radius $R = 10$ fm (the potential goes to zero at distances greater than $3R = 30$ fm). The eigenvalue from (6) for energy $E = -7.72654$ MeV was $\lambda = 0.99997$. The number of grid points used in the calculation was $N_p = N_q = 16, N_{\hat{\boldsymbol{p}}\cdot\hat{\boldsymbol{q}}} = 17$.

The same approach to changing the integration variable can also be applied to calculations of the expectation value of the 3N force. The integrations necessary to carry out this calculation are outlined in Ref. [5] and are practically the same to those used in $\check{A}_{G_0V^{(1)}}$. This allowed the expectation value to be quickly calculated for a number of different 3N states.

IV. NUMERICAL REALIZATION AND RESULTS

Finding the solution to (6) requires the computation of a matrix representation of $\check{A}$ [$\check{A}(E)$ for ^{3}H or $\check{A}(E, R)$ for ^{3}He]. This is achieved using Krylov subspace methods. The procedure starts with an initial set of scalar functions ϕ_0 that satisfy the symmetry conditions $(\phi^{(i)}_{0,tT}(p, q, \hat{\boldsymbol{p}}\cdot\hat{\boldsymbol{q}}) = \pm\phi^{(i)}_{0,tT}(p, q, -\hat{\boldsymbol{p}}\cdot\hat{\boldsymbol{q}})$ where 0 is the index of the initial set of scalar functions ϕ_0) outlined in Ref. [5]. Next, using the Arnoldi algorithm (see, e.g., Sec. 6.2 of Ref. [13]), a finite-sized linear space spanned by N orthonormal vectors $\phi_0, \ldots \phi_{N-1}$ [here the lower index does not correspond to t, T from (4) but only numbers the vectors in the basis] is constructed in such a way that is spans the Krylov subspace $\mathbb{K}$ of operator $\check{A}$:

$$\begin{aligned}&\text{span}(\phi_0, \phi_1, \phi_2, \ldots, \phi_{N-1})\\ &\quad\equiv \mathbb{K} \equiv \text{span}(\phi_0, \check{A}\phi_0, \check{A}^2\phi_0, \ldots, \check{A}^{N-1}\phi_0).\end{aligned} \tag{36}$$

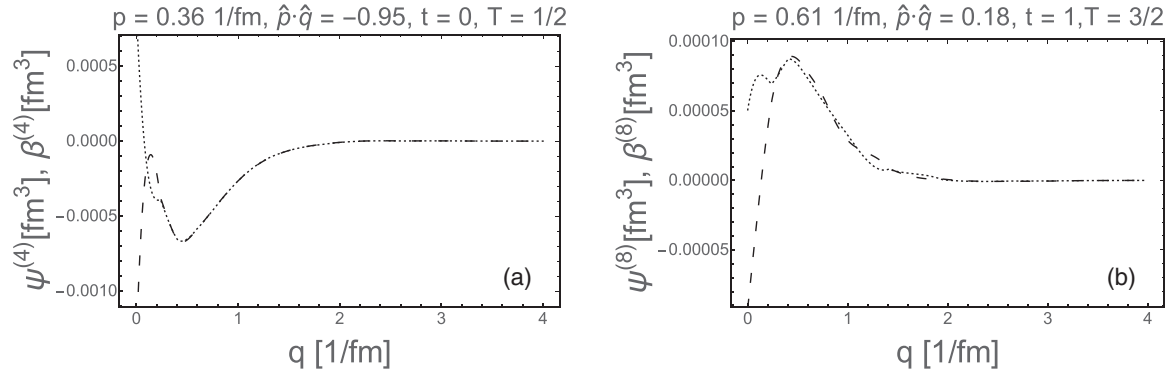

FIG. 4. Similar to (b), (f) from Fig. 3 but the scalar functions were obtained during the first run (see text) with less integration points. Calculations were carried out using both 2N and 3N nuclear forces and a screened Coulomb interaction from Ref. [11] with screening radius $R = 10$ fm (the potential goes to zero at distances greater than $3R = 30$ fm). The eigenvalue from (6) for energy $E = -7.77833$ MeV was $\lambda = 0.99996$.

Simultaneously the matrix elements of $\check{A}$ are calculated within this subspace:

$$(\phi_i, \check{A}\phi_j) \tag{37}$$

thus producing a $N \times N$ matrix representation of $\check{A}$:

$$[\check{A}]_{i=0\ldots N-1\ j=0\ldots N-1} = (\phi_i, \check{A}\phi_j). \tag{38}$$

The Arnoldi algorithm requires the implementation of a scalar product between two sets of scalar functions (37). The spin operators $\check{O}_i(\boldsymbol{p}, \boldsymbol{q})$ (listed in Appendix A) are chosen in such a way that the scalar functions are real allowing the use of:

$$(\gamma, \delta) = \sum_{tTk} \int dpdqdx \gamma_{tT}^{(k)}(p, q, x)\delta_{tT}^{(k)}(p, q, x) \tag{39}$$

as the scalar product for the purposes of the Arnoldi algorithm. In addition to the scalar product all that is required for the Arnoldi algorithm is the implementation of a subroutine that performs the application of $\check{A}$ on the scalar functions. This routine performs the integrals related to the various parts of $\check{A}$ from (8), (9) numerically as described in Secs. III A–III C.

In this paper two values for $N = 80, 110$ were used. This resulted in 80×80 and 110×110 dimensional matrix representations of (6). The FORTRAN LAPACK library was used to solve these equations. Once solved all eigenvalues were discarded except one, whose value was closest to 1 (see λ values given further in the text). The corresponding eigenvector:

$$v = (v_0, \ldots, v_{N-1}) \tag{40}$$

was used to reconstruct the scalar functions from (6) by simple summation:

$$\psi = \sum_{i=0}^{N-1} v_i \phi_i. \tag{41}$$

Solutions ψ calculated for energies E [in $A(E)$ for ^{3}H and $A(E, R)$ in ^{3}He calculations] such that λ is sufficiently close to 1 are good approximations of the solutions to (5). This also means that they are good approximations to the scalar functions of the Faddeev components of the 3N bound state and the bound-state energy is E. Naturally, it is important to verify the obtained solutions and for this reason plots of the scalar functions ψ presented further in this paper also contain the functions β calculated by a single application of $\check{A}$:

$$\beta = \check{A}\psi. \tag{42}$$

A correct solution to (5) implies $\psi = \beta$.

The scalar functions Ψ for the full 3N bound-state wave function are obtained from the scalar functions for the Faddeev component ψ with (for more details see Sec. III A):

$$\Psi = \check{A}_{1+\mathrm{P}}\psi. \tag{43}$$

Using the identity:

$$(\check{1} + \check{P})^2 \equiv 3(\check{1} + \check{P}) \tag{44}$$

an additional simple verification of the calculations can be established. Namely, when $\check{A}_{1+\mathrm{P}}$ is applied to Ψ producing new functions ζ:

$$\zeta = \check{A}_{1+\mathrm{P}}\Psi \tag{45}$$

then (44) implies that $\zeta = 3\Psi$. To check this, all plots of Ψ show also $\frac{1}{3}\zeta$.

The scalar functions ψ, Ψ, β, ζ that were obtained as a result of the Arnoldi algorithm [13] require normalization. A method very similar to the one outlined in Eq. (58) from Ref. [5] was used. This formula can be modified to require only the scalar functions for the full bound state Ψ and this approach was used for all scalar functions.

In the numerical realization scalar functions from (4) are represented using multidimensional arrays. Since three isospin states are considered:

$$\left|\left(t = 0\tfrac{1}{2}\right)T = \tfrac{1}{2}M_T\right\rangle,$$
$$\left|\left(t = 1\tfrac{1}{2}\right)T = \tfrac{1}{2}M_T\right\rangle,$$
$$\left|\left(t = 1\tfrac{1}{2}\right)T = \tfrac{3}{2}M_T\right\rangle,$$

and $i = 1, \ldots, 8$, a set of scalar functions $\phi \equiv \{\phi_{tT}^{(i)}(p, q, \hat{\boldsymbol{p}} \cdot \hat{\boldsymbol{q}})\}$ can be represented using a $3 \times 8 \times N_p \times N_q \times N_{\hat{\boldsymbol{p}}\cdot\hat{\boldsymbol{q}}}$ dimensional array where N_p, N_q are the numbers of grid points for the Jacobi momentum magnitudes and $N_{\hat{\boldsymbol{p}}\cdot\hat{\boldsymbol{q}}}$ is the number of grid points for the angle between the Jacobi momenta.

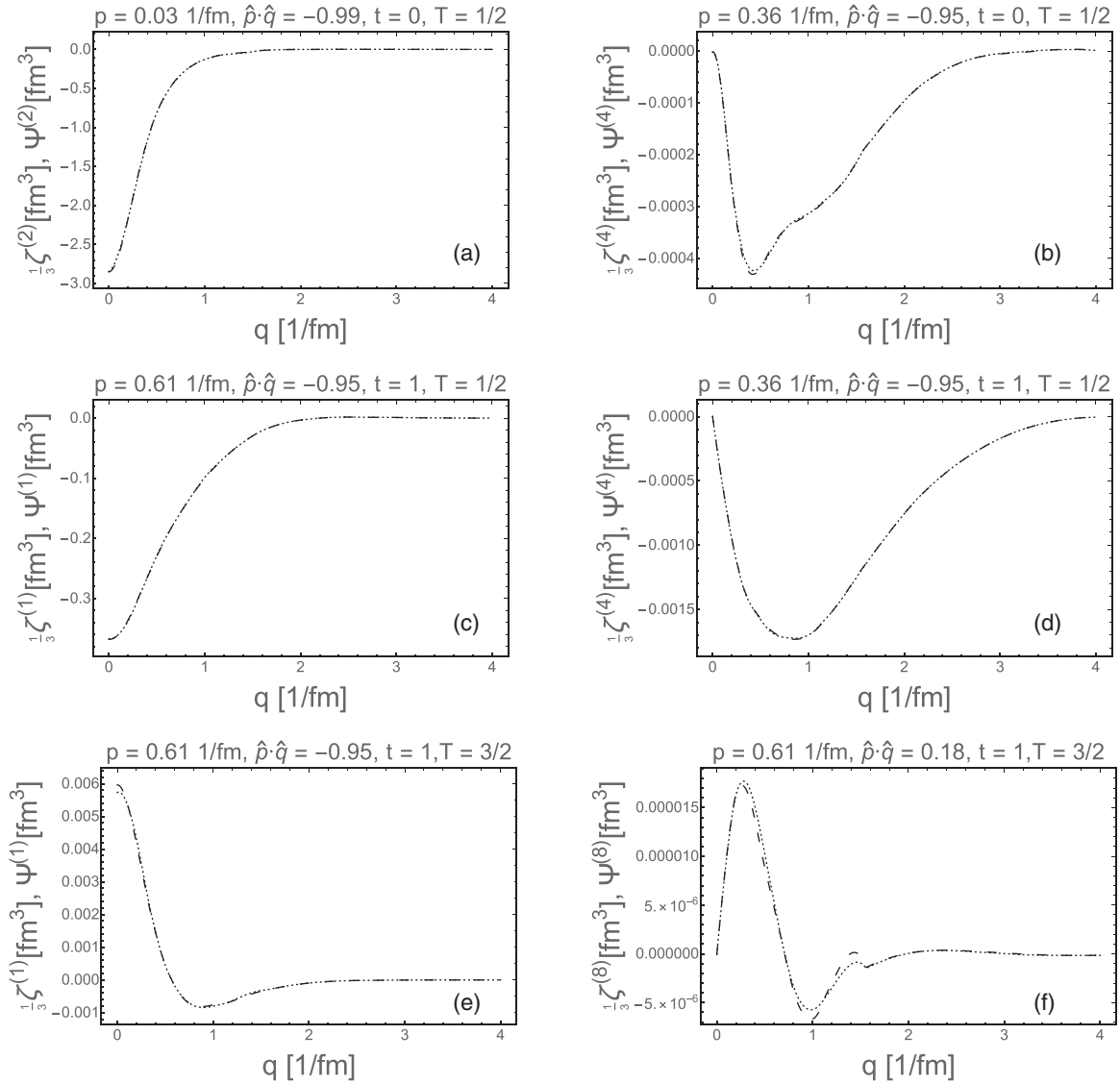

FIG. 5. Selected scalar functions for the ^{3}He bound state. Scalar functions Ψ obtained using (43) are marked using dashed lines while functions $\frac{1}{3}\zeta$ obtained using (45) are marked using dotted lines. Identity (44) implies that $\frac{1}{3}\zeta = \Psi$. Since the lines essentially overlap, with the exception of regions where the value of the function is small, this confirms the reconstruction of the bound state scalar functions. Plots (a), (b) contain the $t = 0, T = \frac{1}{2}$ isospin component; (c), (d) contain the $t = 1, T = \frac{1}{2}$ isospin component; and (e), (f) contain the $t = 1, T = \frac{3}{2}$ isospin component. Calculations were performed during the second run (see text) with improved numerics and using both 2N and 3N nuclear forces and a screened Coulomb interaction from Ref. [11] with screening radius $R = 10$ fm (the potential goes to zero at distances greater than $3R = 30$ fm). The eigenvalue from (6) for energy $E = -7.72654$ MeV was $\lambda = 0.99997$. The number of grid points used in the calculation was $N_p = N_q = 16, N_{\hat{p}\cdot\hat{q}} = 17$.

Two different values for the number of lattice points N_p, N_q, $N_{\hat{p}\cdot\hat{q}}$ were used in calculations presented in this paper in what will be referred to as the first and second run. In the first run of the code $N_p = N_q = N_{\hat{p}\cdot\hat{q}} = 16$ was used and in the second run $N_{\hat{p}\cdot\hat{q}}$ was changed to 17. This change was dictated by the different computer architecture used in the second set of calculations.

In the second run, an improvement in numerical precision was achieved by increasing the number of Gaussian integration points for the azimuthal angle in Eq. (26) from 16 to 64, the number of iterations in the Arnoldi algorithm was increased from $N = 80$ to $N = 110$ and the range of lattice points for q was changed from $q < 5$ fm^{-1} to $q < 4$ fm^{-1}. The range of lattice points for p remained unchanged $p < 5$ fm^{-1}. These combined changes resulted in a visible increase in the quality of the results as will be shown in plots presented in this section. The currently obtained results encourage the adaptation of two-stage parallelization in order to optimize the code for the new JURECA Booster [14] computer. This would allow calculations with an increased number of N_p, N_q, $N_{\hat{p}\cdot\hat{q}}$ grid points, but is reserved for future calculations that will be performed with more modern chiral potentials. Current calculations are performed with a relatively small number of grid points and use the same, first generation, chiral NNLO 2N

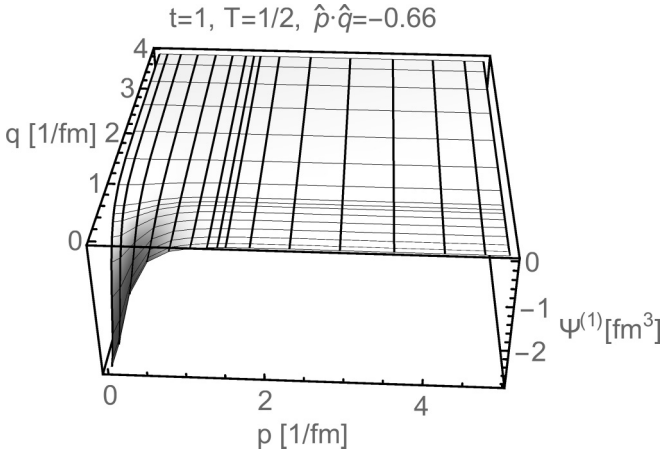

FIG. 6. Dominant scalar function for the ^{3}He bound state plotted as a function of the magnitude of the Jacobi momenta p, q for a chosen value of $\hat{\boldsymbol{p}} \cdot \hat{\boldsymbol{q}}$.

and 3N potentials as in Ref. [5]. In this paper, however, both the proton-proton and neutron-proton versions of the 2N force are used and a third $T = \frac{3}{2}$ isospin component is incorporated into the calculations. Moreover a new integration scheme is used in the implementation of the 3N force that significantly reduces the numerical work needed to run the code.

The benefit of this new method of carrying out the integrals related to the 3N force can be demonstrated by considering Fig. 2. The plots show the dependence of the ^{3}He bound-state energy on the screening radius of the screened Coulomb interaction from Ref. [11]. Figures 2(a)–2(e) show the eigenvalue λ from (6) that is closest to 1 as a function of the energy E. These five plots correspond to screening radii $R = 1, 2, 4, 7.5, 10$ fm and the data was obtained during the first run. The amount of numerical work required to compute a single point from Figs. 2(a)–2(e) using the old method of carrying out 3N integrals from Ref. [5] is comparable to the amount of work needed to calculate all points from these plots using the new method outlined in Sec. III C. The reason behind this improvement lies in the implementation of the 3N force, which is the most expensive part of the calculation. Using the new method a significant portion of the integrals can be performed once and then later reused making Arnoldi iterations with 2N and 3N potentials not much more expensive than calculations that use only 2N forces.

The $\lambda(E)$ dependence in Fig. 2 is visibly linear and a simple linear fit was used to extrapolate the bound-state energy E_{BS} such that $\lambda(E_{BS}) = 1$. The E_{BS} dependence on the screening radius R is shown on Fig. 2(f). The difference between the extrapolated bound-state energy for $R = 7.5$ fm and $R = 10$ fm is minimal and in the second run of the calculations a single value $R = 10$ fm was used. The screened Coulomb potential $\omega_R(r)$ from Ref. [11] is a piecewise function, whose domain is divided into three parts $0 - R$, $R - 3R$, $3R - \infty$ and it goes to zero at distances r greater than $3R = 30$ fm. An additional benefit of using this potential is that the analytical momentum space expression for the screened Coulomb force is worked out and does not require additional numerical work. In the second run a similar procedure was used to obtain the scalar functions for the bound states. A range of energies was scanned looking for $\lambda = 1$, next a linear fit was used to extrapolate to the bound-state energy.

Figure 3 shows selected scalar functions for the Faddeev component of the ^{3}He bound state obtained during the second run. All plots contain both the ψ functions from (5) [that were reconstructed using (41)] and the β functions from (42). The obtained values of these functions practically overlap, verifying the solution. The additional $T = \frac{3}{2}$ component is visible on Figs. 3(e) and 3(f). In Fig. 4 selected scalar functions obtained during the first run are shown. When these two plots, Figs. 4(a) and 4(b), are compared with Figs. 3(b) and 3(f) numerical artifacts are visible for low values of q. The disappearance of these artifacts in the second run is indicative of the positive effects of the changes made in the second run of calculations. It should, however, be noted that the numerical artifacts observed in the first run affect only the nondominant scalar functions whose values are relatively very small. For this reason they are not expected to have a significant impact on the extrapolated bound-state energy and other observables.

Figure 5 shows selected scalar functions Ψ for the full ^{3}He bound state obtained using (43) during the second run. All plots also contain the $\frac{1}{3}\zeta$ functions from (45). The values of these two functions practically overlap again verifying the numerical realization. Differences appear for nondominant

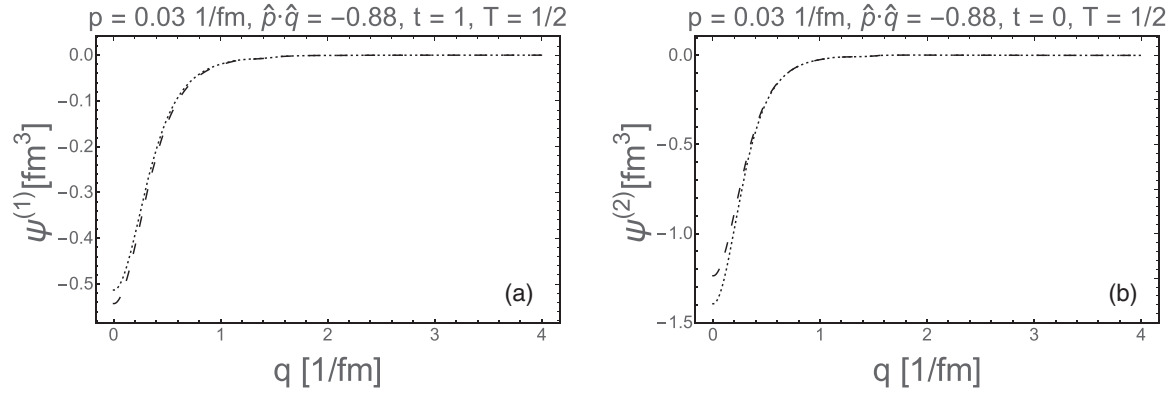

FIG. 7. Similar to Fig. 3. Comparison of two dominant scalar functions [(a) : $\psi^{(1)}$, (b) : $\psi^{(2)}$] for the Faddeev component of ^{3}H and ^{3}He. Dashed lines correspond to ^{3}H and dotted lines correspond to ^{3}He.

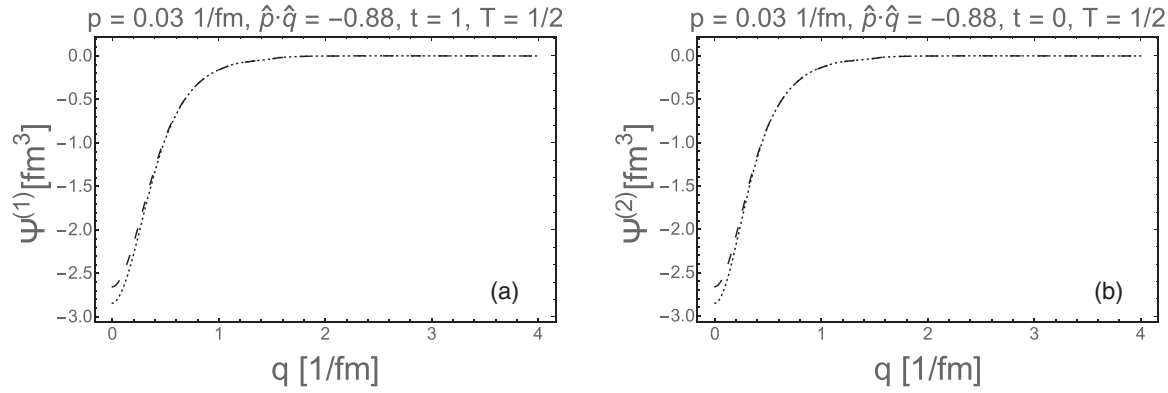

FIG. 8. Similar to Fig. 5. Comparison of two dominant scalar functions [(a) : $\Psi^{(1)}$, (b) : $\Psi^{(2)}$] for the ^{3}H and ^{3}He bound state. Dashed lines correspond to ^{3}H and dotted lines correspond to ^{3}He.

scalar functions and at low values of the momenta and angles. These differences can be attributed to problems with interpolations in regions close to the function domain boundaries and are barely visible in Fig. 5 where the same values of p and $\hat{\boldsymbol{p}}\cdot\hat{\boldsymbol{q}}$ were used as in Fig. 3 for the purpose of comparison. Figure 6 exemplifies the dependence of the dominant, first, scalar function $\Psi^{(1)}$ for the full ^{3}He bound state on the magnitude of both Jacobi momenta p, q for a given angle $\hat{\boldsymbol{p}}\cdot\hat{\boldsymbol{q}}$. It can be observed that the scalar function quickly drops to zero in a region where the momenta are greater than $\approx 2[\frac{1}{\text{fm}}]$.

The differences between the two dominant Faddeev component scalar functions ψ are shown in Fig. 7 for ^{3}He and ^{3}H. In both Figs. 7(a) and 7(b) the $T = \frac{1}{2}$ components are dominant. This dominance is also clearly visible in Figs. 8(a) and 8(b) that contain the largest scalar functions Ψ for the full wave function of ^{3}H and ^{3}He. Finally in Fig. 9 two dominant scalar functions Ψ for the ^{3}He bound state calculated with a 3N force and without a 3N force are compared. The largest differences appear for the $T = \frac{1}{2}$ components.

Table I contains a comparison of the energy, eigenvalue closest to 1 [see Eq. (6)] and expectation values of the 2N potential and kinetic energies. These values were calculated using the ^{3}H wave function obtained using the 3D approach and standard partial wave techniques without a 3N potential and using two different versions of the 2N force. The three-dimensional (3D) results and the first set of the partial wave results (PWD 1) were obtained using the neutron-proton and neutron-neutron versions of the 2N interaction (the neutron-neutron potential was approximated by the available proton-proton force). The second set of the partial wave results (PWD 2) were obtained using only the neutron-proton version of the 2N force, the same interaction as was used in Ref. [5]. The aim of this comparison is to verify the use of the new 2N interaction that takes into account two different isospin cases (neutron-proton and neutron-neutron). Since the values of the first set of partial wave results (PWD 1) agree with the three-dimensional results (3D) the new 2N potential is used in further calculations. The small differences in expectation values can be attributed to the slightly different eigenvalues and to the lack of the $T = \frac{3}{2}$ isospin component in the partial wave calculations. A larger energy difference can be observed between the first two columns (3D, PWD 1) and the third column (PWD 2). This shift in energy can be attributed to the change of the 2N force.

Table II contains a comparison of the energy, eigenvalue closest to 1 and expectation values of the 2N potential, 3N potential, and kinetic energies for ^{3}H calculated with a 3N interaction. The second and third column (3D 1, PWD [5])

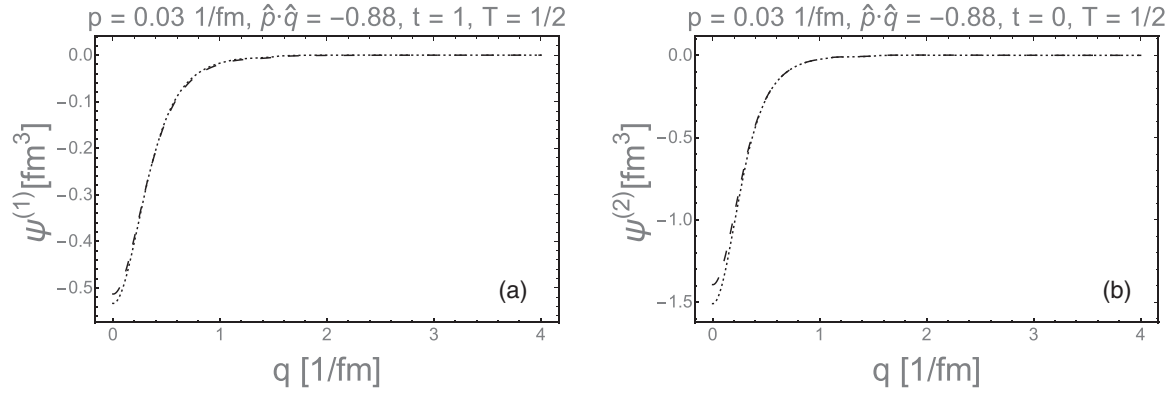

FIG. 9. Similar to Fig. 3. Comparison of two dominant scalar functions for the ^{3}He Faddeev component calculated with and without the 3N force. Dashed lines were calculated with the use of the 3N interaction and dotted lines were calculated with only 2N forces. In calculations without the 3N force the eigenvalue from (6) for energy $E = -7.34124$ MeV was $\lambda = 0.99997$.

TABLE I. In MeV: the ^{3}H bound-state energy E the expectation value of the kinetic energy $\langle E_{\rm kin}\rangle$, the expectation value of the 2N potential $\langle E^{2N}_{\rm pot}\rangle$, and $\Sigma = \langle E_{\rm kin}\rangle + \langle E^{2N}_{\rm pot}\rangle$. The eigenvalue λ closest to 1 in Eq. (6) is in the last row. 3D calculations obtained during the second run (see text) are in the first column (3D). The second column (PWD 1) contains analogous results but obtained using standard partial wave techniques and without the $T = 3/2$ isospin component. The third column (PWD 2) contains partial wave results that use only the neutron-proton version of the two nucleon potential. Additionally, for the 3D results, the expectation value of the screened Coulomb interaction: 0.71 MeV and 3N force: 0.06 MeV was calculated.

	3D	PWD 1	PWD 2
E	−8.02	−8.07	−8.31
$\langle E_{\rm kin}\rangle$	31.32	31.57	31.99
$\langle E^{2N}_{\rm pot}\rangle$	−39.29	−39.62	−40.28
Σ	−7.97	−8.05	−8.29
λ	0.99997	0.99949	0.9995

contain values that were calculated in Ref. [5] using the 3D approach and the standard partial wave approach. These results were calculated using only the neutron-proton version of the 2N potential. The first column (3D) contains new results obtained using the more efficient implementation of the 3N force described in Sec. III C and a 2N potential that distinguishes between the neutron-proton and neutron-neutron cases. Similarly as in Table I there is a roughly 0.25 MeV shift in the energy E between the new results (3D) and old results from Ref. [5] (3D [5], PWD [5]) that can be attributed to the different 2N forces. The expectation values of the 3N force are similar in all three columns. This encourages the use of the new 3N force implementation in further calculations.

TABLE II. In MeV: the ^{3}H bound-state energy E, the expectation value of the kinetic energy $\langle E_{\rm kin}\rangle$, the expectation value of the 2N potential $\langle E^{2N}_{\rm pot}\rangle$, the expectation value of the 3N potential $\langle E^{3N}_{\rm pot}\rangle$, and $\Sigma = \langle E_{\rm kin}\rangle + \langle E^{2N}_{\rm pot}\rangle + \langle E^{3N}_{\rm pot}\rangle$. The eigenvalue λ closest to 1 in Eq. (6) is in the last row. 3D calculations obtained during the second run (see text) using both 2N and 3N forces are in the first column (3D). The second column (3D 1) contains 3D results that used the same 3N force and the same neutron-proton version of the 2N force as in Ref. [5] (this calculation includes the $T = 3/2$ isospin component but its influence is negligible). The second column (3D 1) can be compared with the third column (PWD [5]), which contains partial wave results from Ref. [5] obtained using the same potentials as column two and not including the $T = 3/2$ component. Additionally, the expectation value of the 2N screened Coulomb interaction was calculated for the newest 3D calculations: 0.71 MeV.

	3D	3D 1	PWD [5]
E	−8.40	−8.62	−8.646
$\langle E_{\rm kin}\rangle$	32.91	33.25	33.448
$\langle E^{2N}_{\rm pot}\rangle$	−40.45	−41.02	−41.329
$\langle E^{3N}_{\rm pot}\rangle$	−0.79	−0.78	−0.765
Σ	−8.33	−8.55	−8.646
λ	0.99998	0.99998	1.0

TABLE III. In MeV: the ^{3}He bound-state energy E, the expectation value of the kinetic energy $\langle E_{\rm kin}\rangle$, the expectation value of the strong 2N potential $\langle E^{2N}_{\rm pot}\rangle$, the expectation value of the screened Coulomb potential $\langle E^{2N}_{C}\rangle$ and $\Sigma = \langle E_{\rm kin}\rangle + \langle E^{2N}_{\rm pot}\rangle + \langle E^{2N}_{C}\rangle$. These values were obtained from ^{3}He bound-state scalar functions obtained during the second run (see text). The bound state was calculated using only 2N forces. Additionally, the expectation value of the 3N force was calculated: 0.04 MeV.

E	−7.34
$\langle E_{\rm kin}\rangle$	30.73
$\langle E^{2N}_{\rm pot}\rangle$	−38.70
$\langle E^{2N}_{C}\rangle$	0.70
Σ	−7.27
λ	0.99997

Other differences across the three cases can be attributed to a smaller number of N_p, N_q, $N_{\hat{\mathbf{p}}\cdot\hat{\mathbf{q}}}$ points used in the newest calculation and to the lack of the $T = \frac{3}{2}$ isospin component in calculations from Ref. [5].

The next set of results in Tables III and IV are related to ^{3}He calculated without and with the 3N potential, respectively. In both cases a significant contribution to the total energy comes from the screened Coulomb potential. It should be noted that the calculations in Table IV would not be practically possible with the old implementation of the 3N force used in Ref. [5] due to the large numerical cost. The reason for this is that the ^{3}He calculations have to be repeated for many different energies when looking for an energy value such that the eigenvalue from Eq. (6) is sufficiently close to 1. This was demonstrated in Figs. 2(a)–2(e). The new implementation from Sec. III C, after carrying out some initial numerical work, makes Arnoldi iterations with both 2N and 3N forces not significantly more expensive than iterations with only

TABLE IV. In MeV: the expectation values for the kinetic energy ($E_{\rm kin}$), the strong 2N potential ($E^{2N}_{\rm pot}$), the screened Coulomb interaction (E^{2N}_{C}), and the 3N force ($E^{3N}_{\rm pot}$). These values were obtained from ^{3}He bound-state scalar functions obtained during the second run (see text). The bound state was calculated using both 2N and 3N forces. The eigenvalue from (6) for energy $E = -7.72654$ MeV was $\lambda = 0.99997$.

E	−7.73
$\langle E_{\rm kin}\rangle$	32.36
$\langle E^{2N}_{\rm pot}\rangle$	−39.91
$\langle E^{2N}_{C}\rangle$	0.69
$\langle E^{3N}_{\rm pot}\rangle$	−0.77
Σ	−7.63
λ	0.99997

TABLE V. Nonzero matrix elements of the Fermi current for particle 1. The spin projection of the triton in the initial state is m_i and the spin projection of helium-3 in the final state is m_f.

matrix element	value
$\langle {}^3\text{He}\ m_f = -\frac{1}{2}\vert\check{\rho}_F(1)\vert{}^3\text{H}\ m_i = -\frac{1}{2}\rangle$	0.332825
$\langle {}^3\text{He}\ m_f = \frac{1}{2}\vert\check{\rho}_F(1)\vert{}^3\text{H}\ m_i = \frac{1}{2}\rangle$	0.332825

2N forces. Figure 2(f) shows that it is sufficient to use the screened Coulomb potential [11] with screening radius 10 fm and this value was used in the results from Tables III and IV.

The obtained ^{3}H and ^{3}He wave functions were the starting point used to calculate matrix elements necessary to describe triton β decay. These elements were calculated for two simple single-nucleon current models. Details of this calculation are available in Appendix B. Numerical values for the matrix elements of the Fermi current for particle one:

$$\langle \boldsymbol{k}_1'|\check{\rho}_F(1)|\boldsymbol{k}_1\rangle = \check{\tau}(1)_+\,\check{1}, \tag{46}$$

where $\boldsymbol{k}_1'$, $\boldsymbol{k}$ are the momenta of particle one in the final and initial states, $\check{\tau}(1)_+$ is the isospin raising operator and $\check{1}$ is the identity operator in the spin space of particle one, are gathered in Table V.

Matrix elements for the z component of the Gamow-Teller current:

$$\langle \boldsymbol{k}_1'|\check{\boldsymbol{j}}_{GTz}(1)|\boldsymbol{k}_1\rangle = \check{\tau}(1)_+\,\check{\sigma}(1)_z, \tag{47}$$

where $\check{\sigma}(1)_z$ is a component of the vector spin operator $\check{\boldsymbol{\sigma}}(1) = (\check{\sigma}(1)_x, \check{\sigma}(1)_y, \check{\sigma}(1)_z)$, are gathered in Table VI. In order to verify these results several additional calculations were performed. First, matrix elements of (47) were calculated with $\check{\sigma}(1)_z$ replaced by the spherical components of the spin $\check{\sigma}(1)_{+1}$, $\check{\sigma}(1)_{-1}$:

$$\check{j}_{GT+}(1) = \check{\tau}(1)_+\check{\sigma}(1)_{+1}, \tag{48}$$

$$\check{j}_{GT-}(1) = \check{\tau}(1)_+\check{\sigma}(1)_{-1}. \tag{49}$$

These results are gathered in Table VII. Since observables are proportional to the sum over the spin projections in the initial and final states m_i, m_f:

$$S(\check{j}) = \sum_{m_f=\pm\frac{1}{2}}\sum_{m_i=\pm\frac{1}{2}} |\langle {}^3\text{He}\ m_f|\check{j}(1)|{}^3\text{H}\ m_i\rangle|^2 \tag{50}$$

this sum was calculated for $\check{\sigma}(1)_z$, $\check{\sigma}(1)_{+1}$, and $\check{\sigma}(1)_{-1}$ and compared in Table VIII. The values are essentially the same and this confirms the correctness of the calculations from Tables VI and VII. Next, the expectation values of the $\frac{1}{2}[\check{1} + \check{\tau}(1)_3]$ isospin operator [$\check{\tau}(1)_3$ is the third component of

TABLE VI. Nonzero matrix elements of the Gamow-Teller current for particle 1. The spin projection of the triton in the initial state is m_i and the spin projection of helium-3 in the final state is m_f.

matrix element	value
$\langle {}^3\text{He}\ m_f = -\frac{1}{2}\vert\check{j}_{GTz}(1)\vert{}^3\text{H}\ m_i = -\frac{1}{2}\rangle$	0.310749
$\langle {}^3\text{He}\ m_f = \frac{1}{2}\vert\check{j}_{GTz}(1)\vert{}^3\text{H}\ m_i = \frac{1}{2}\rangle$	−0.310749

TABLE VII. Nonzero matrix elements of the currents from (48) and (49). The spin projection of the triton in the initial state is m_i and the spin projection of helium-3 in the final state is m_f.

matrix element	value
$\langle {}^3\text{He}\ m_f = \frac{1}{2}\vert\check{j}_{GT+}(1)\vert{}^3\text{H}\ m_i = -\frac{1}{2}\rangle$	0.439465
$\langle {}^3\text{He}\ m_f = -\frac{1}{2}\vert\check{j}_{GT-}(1)\vert{}^3\text{H}\ m_i = \frac{1}{2}\rangle$	−0.439465

the isospin for particle 1] were calculated. The obtained values were 0.666395 for ^{3}He and 0.333533 for ^{3}H. These two results provide an additional verification since they are very close to $\frac{2}{3}$ and $\frac{1}{3}$ that could be expected for ^{3}He and ^{3}H, respectively. Results for simple single-nucleon currents that are presented here, open up the possibility to perform calculations with more complicated models and two-nucleon currents.

V. SUMMARY AND OUTLOOK

This paper shows that three-nucleon bound-state calculations with screened Coulomb potentials are possible using the three-dimensional approach. Instead of relying on the partial wave decomposition of operators relevant to the calculation, the new approach uses the three-dimensional momentum degrees of freedom of the nucleons directly. A practical numerical realization of these calculations is made feasible by the idea to write the three-nucleon state as a linear combination of spin operators and scalar functions. These scalar functions effectively define the state and are the central object in the three-dimensional calculations.

The dependency of the ^{3}He bound-state energy on the screening radius of the Coulomb interaction was shown and it was determined that it is sufficient to perform calculations with a screening radius of 10 [fm] (for the model of Coulomb interaction used this means that the potential goes to zero at distances larger than 30 [fm]). At this radius the values of observables are expected to be converged. Plots showing selected scalar functions were given. Apart from the scalar functions that define the bound state, the plots also contain additional, overlapping, functions that verify the validity of the obtained solution. It should be noted that the new implementation of the three-nucleon force in the three-dimensional calculations was crucial for ^{3}He calculations by significantly reducing the numerical work required for the calculations.

TABLE VIII. Values of the sum from (50) for currents (47)–(49). The values are essentially the same for all cases. Since observables are proportional to (50) [among other things, the proportionality coefficients contain a factor of $3^2 = 9$ stemming from the necessity to use $\check{j}(1) + \check{j}(2) + \check{j}(3)$] this verifies the calculation in Tables VI and VII.

sum	value
$S(\check{j}_{GTz})$	0.19313
$S(\check{j}_{GT+})$	0.19313
$S(\check{j}_{GT-})$	0.19313

Having calculated the bound states of ^{3}He and ^{3}H, the expectation values of the kinetic and potential energies were calculated. This further confirmed the correctness of the obtained results but also showed that it would be beneficial to perform the calculations using a greater number of grid points to represent the scalar functions. Calculations with an increased number of points are planned for more modern models of chiral two- and three- nucleon interactions.

Additionally, basic matrix elements related to the triton β decay were calculated. These matrix elements are based on simple models of nuclear currents and can be directly used to calculate observables related to that decay.

ACKNOWLEDGMENTS

The author would like to thank J. Golak, H. Witała, and R. Skibiński from the Jagiellonian University for their advice and help in preparing this paper as well as A. Nogga from Forschungszentrum Jüelich for very fruitful discussions. The project was financed from the resources of the National Science Center, Poland, under Grants No. 2016/22/M/ST2/00173 and No. 2016/21/D/ST2/01120. Numerical calculations were preformed on the supercomputer clusters of the Jülich Supercomputing Center, Jülich, Germany.

APPENDIX A: SPIN OPERATORS IN 3N OPERATOR FORM

Below is a list of spin operators used in the operator form of the 3N (Faddeev, bound) state (4). Spin operators acting in the spaces of particle 1, 2, 3 are denoted as $\check{\boldsymbol{\sigma}}(1)$, $\check{\boldsymbol{\sigma}}(2)$, $\check{\boldsymbol{\sigma}}(3)$, respectively, and $\check{\boldsymbol{\sigma}}(2,3) = \frac{1}{2}[\check{\boldsymbol{\sigma}}(2) - \check{\boldsymbol{\sigma}}(3)]$. Vectors $\boldsymbol{p}$, $\boldsymbol{q}$ are the Jacobi momenta of the 3N system (if $\boldsymbol{k}_{1,2,3}$ are individual particle momenta then $\boldsymbol{p} = \frac{1}{2}(\boldsymbol{k}_2 - \boldsymbol{k}_3)$, $\boldsymbol{q} = \frac{2}{3}[\boldsymbol{k}_1 - \frac{1}{2}(\boldsymbol{k}_2 + \boldsymbol{k}_3)]$).

$$\check{O}_1(\boldsymbol{p},\boldsymbol{q}) = \check{1},$$

$$\check{O}_2(\boldsymbol{p},\boldsymbol{q}) = \frac{1}{\sqrt{3}}\check{\boldsymbol{\sigma}}(2,3)\cdot\check{\boldsymbol{\sigma}}(1),$$

$$\check{O}_3(\boldsymbol{p},\boldsymbol{q}) = \sqrt{\frac{3}{2}}\frac{1}{i}\check{\boldsymbol{\sigma}}(1)\cdot(\hat{\boldsymbol{p}}\times\hat{\boldsymbol{q}}),$$

$$\check{O}_4(\boldsymbol{p},\boldsymbol{q}) = \frac{1}{\sqrt{2}}(i\check{\boldsymbol{\sigma}}(2,3)\cdot(\hat{\boldsymbol{p}}\times\hat{\boldsymbol{q}}) - (\check{\boldsymbol{\sigma}}(1)\times\check{\boldsymbol{\sigma}}(2,3))\cdot(\hat{\boldsymbol{p}}\times\hat{\boldsymbol{q}})),$$

$$\check{O}_5(\boldsymbol{p},\boldsymbol{q}) = \frac{1}{i}\Big(\check{\boldsymbol{\sigma}}(2,3)\cdot(\hat{\boldsymbol{p}}\times\hat{\boldsymbol{q}}) - \frac{i}{2}(\check{\boldsymbol{\sigma}}(1)\times\check{\boldsymbol{\sigma}}(2,3))\cdot(\hat{\boldsymbol{p}}\times\hat{\boldsymbol{q}})\Big),$$

$$\check{O}_6(\boldsymbol{p},\boldsymbol{q}) = \sqrt{\frac{3}{2}}\Big(\check{\boldsymbol{\sigma}}(2,3)\cdot\hat{\boldsymbol{p}}\check{\boldsymbol{\sigma}}(1)\cdot\hat{\boldsymbol{p}} - \frac{1}{3}\check{\boldsymbol{\sigma}}(2,3)\cdot\check{\boldsymbol{\sigma}}(1)\Big),$$

$$\check{O}_7(\boldsymbol{p},\boldsymbol{q}) = \sqrt{\frac{3}{2}}\Big(\check{\boldsymbol{\sigma}}(2,3)\cdot\hat{\boldsymbol{q}}\check{\boldsymbol{\sigma}}(1)\cdot\hat{\boldsymbol{q}} - \frac{1}{3}\check{\boldsymbol{\sigma}}(2,3)\cdot\check{\boldsymbol{\sigma}}(1)\Big),$$

$$\check{O}_8(\boldsymbol{p},\boldsymbol{q}) = \frac{3}{2}\frac{1}{\sqrt{5}}\Big(\check{\boldsymbol{\sigma}}(2,3)\cdot\hat{\boldsymbol{q}}\check{\boldsymbol{\sigma}}(1)\cdot\hat{\boldsymbol{p}} + \check{\boldsymbol{\sigma}}(2,3)\cdot\hat{\boldsymbol{p}}\check{\boldsymbol{\sigma}}(1)\cdot\hat{\boldsymbol{q}} - \frac{2}{3}\hat{\boldsymbol{p}}\cdot\hat{\boldsymbol{q}}\check{\boldsymbol{\sigma}}(2,3)\cdot\check{\boldsymbol{\sigma}}(1)\Big),$$

APPENDIX B: MATRIX ELEMENTS RELATED TO THE TRITON β DECAY

The calculation of observables related to the β decay process:

$$^3\mathrm{H} \to {}^3\mathrm{He} + e + \bar{\nu}_e$$

requires computing matrix elements of the form:

$$\langle\Psi_{^3\mathrm{He}}|\check{j}(i)|\Psi_{^3\mathrm{H}}\rangle, \tag{B1}$$

where $\check{j}(i=1,2,3)$ is the single-nucleon current acting in the space of nucleon i. In this paper two simple current models are used:

$$\langle\boldsymbol{k}_i'|\check{j}_{GT}(i)|k_i\rangle = \check{\tau}_i^+\check{\sigma}(i)_z := \check{\tau}_i^+\check{f}_{GT}(\boldsymbol{k}_i',\boldsymbol{k}_i), \tag{B2}$$

and

$$\langle\boldsymbol{k}_i'|\check{\rho}_F(i)|\boldsymbol{k}_i\rangle = \check{\tau}_i^+\check{1} := \check{\tau}_i^+\check{f}_F(\boldsymbol{k}_i',\boldsymbol{k}_i), \tag{B3}$$

where on the right-hand side the dependence on single-particle momentum in the initial and final state was added for generality. In Eqs. (B2) and (B3) $\check{\tau}_i^+$ is the isospin raising operator for particle i, $\check{\sigma}(i)_z$ is the z component of the spin operator for particle i, $\check{1}$ is the identity operator in spin space and $\boldsymbol{k}_i'$, $\boldsymbol{k}_i$ are the momenta of particle i in the final and initial states.

Using the property:

$$\langle\boldsymbol{k}_1',\boldsymbol{k}_2',\boldsymbol{k}_3'|\check{j}(1)|\boldsymbol{k}_1,\boldsymbol{k}_2,\boldsymbol{k}_3\rangle = \check{f}(\boldsymbol{k}_1',\boldsymbol{k}_1)\delta^3(\boldsymbol{k}_2'-\boldsymbol{k}_2)\delta^3(\boldsymbol{k}_3'-\boldsymbol{k}_3),$$

and the relation between the single-particle momentum eigenstates and Jacobi momentum eigenstates:

$$\langle\boldsymbol{k}_1\boldsymbol{k}_2\boldsymbol{k}_3|\boldsymbol{p}\boldsymbol{q}\boldsymbol{K}\rangle = \delta^3\big(\boldsymbol{p} - \tfrac{1}{2}(\boldsymbol{k}_2-\boldsymbol{k}_3)\big) \times \delta^3\big(\boldsymbol{q} - \tfrac{2}{3}\big(\boldsymbol{k}_1 - \tfrac{1}{2}(\boldsymbol{k}_2+\boldsymbol{k}_3)\big)\big) \times \delta^3(\boldsymbol{K} - \boldsymbol{k}_1 - \boldsymbol{k}_2 - \boldsymbol{k}_3),$$

where $\boldsymbol{K}$ is the total momentum of the 3N system, the operator form of the ^{3}He and triton bound states from (4), the assumption that the total momentum of the 3N system does not change in the triton β decay process and that initially the triton is at rest it is possible to write (B1) for particle $i=1$ as:

$$\langle\Psi_{^3\mathrm{He}},m_f|\check{j}(1)|\Psi_{^3\mathrm{H}},m_i\rangle = \int d^3\boldsymbol{p}d^3\boldsymbol{q}\sum_{t'T'}\sum_{tT}\left\langle\left(t'\frac{1}{2}\right)T'M_{T'}\middle|\check{\tau}_1^+\middle|\left(t\frac{1}{2}\right)TM_T\right\rangle\sum_{i=1}^{8}\sum_{j=1}^{8}\Psi^{(i)}_{^3\mathrm{He};t'T'}(p,q,\hat{\boldsymbol{p}}\cdot\hat{\boldsymbol{q}})\Psi^{(j)}_{^3\mathrm{H};tT}(p,q,\hat{\boldsymbol{p}}\cdot\hat{\boldsymbol{q}}) \times\langle\chi_{m_f}|\check{O}_j(\boldsymbol{p}',\boldsymbol{q}')^\dagger\check{f}(\boldsymbol{k}_1'=\boldsymbol{q},\boldsymbol{k}_1=\boldsymbol{q})\check{O}_i(\boldsymbol{p}',\boldsymbol{q}')|\chi_{m_i}\rangle \tag{B4}$$

where m_f, m_i are spin projections of the 3N system in the final and initial state and $\Psi_{^3\mathrm{He}}$, $\Psi_{^3\mathrm{H}}$ are scalar functions that determine the ^{3}He and ^{3}H bound states, respectively.

The integral in Eq. (B4) can be easily calculated using a similar choice of integral variables as in Sec. III C:

$$\boldsymbol{p} = p\check{R}^{\phi_p}_{\hat{z}}\check{R}^{\theta_p}_{\hat{y}}(0,0,1),$$

$$\boldsymbol{q} = q\check{R}^{\phi_p}_{\hat{z}}\check{R}^{\theta_p}_{\hat{y}}\check{R}^{\phi_q}_{\hat{z}}\check{R}^{\theta_q}_{\hat{y}}(0,0,1).$$

Choosing this parametrization leads to $\hat{\boldsymbol{p}}\cdot\hat{\boldsymbol{q}} = \cos(\theta_q) := x_{\boldsymbol{q}}$. This can be used to greatly simplify (B4) to the following expression:

$$\begin{aligned}\langle \Psi_{^3\mathrm{He}}, m_f|\check{j}(1)|\Psi_{^3\mathrm{H}}, m_i\rangle = &\int_0^\infty dpp^2\int_0^\infty dqq^2\int_{-1}^1 dx_{\boldsymbol{q}}\sum_{t'T'}\sum_{tT}\left\langle\left(t'\frac{1}{2}\right)T'M_{T'}\middle|\check{\tau}_1^+\middle|\left(t\frac{1}{2}\right)TM_T\right\rangle\\ &\times\sum_{i=1}^8\sum_{j=1}^8\Psi^{(i)}_{^3\mathrm{He};t'T'}(p,q,x_{\boldsymbol{q}})\Psi^{(j)}_{^3\mathrm{H};tT}(p,q,x_{\boldsymbol{q}})\\ &\times\left\{\int_0^\pi d\theta_{\boldsymbol{p}}\sin(\theta_{\boldsymbol{p}})\int_0^{2\pi}d\phi_{\boldsymbol{p}}\int_0^{2\pi}d\phi_{\boldsymbol{q}}\langle\chi_{m_f}|\check{O}_j(\boldsymbol{p},\boldsymbol{q})^\dagger\check{f}(\boldsymbol{k}_1'=\boldsymbol{q},\boldsymbol{k}_1=\boldsymbol{q})\check{O}_i(\boldsymbol{p},\boldsymbol{q})|\chi_{m_i}\rangle\right\},\end{aligned}$$

where the integrals in the curly brackets can be computed once and then used in calculations with different scalar functions Ψ.

[1] S. Bayegan, M. R. Hadizadeh, and M. Harzchi, Phys. Rev. C **77**, 064005 (2008).

[2] M. A. Shalchi and S. Bayegan, Eur. Phys. J. A **48**, 6 (2012).

[3] W. Glöckle, Ch. Elster, J. Golak, R. Skibiński, H. Witała, and H. Kamada, Few-Body Syst. **47**, 25 (2010).

[4] H. Witała, J. Golak, R. Skibiński, and K. Topolnicki, J. Phys. G **41**, 094011 (2014).

[5] J. Golak, K. Topolnicki, R. Skibiński, W. Glöckle, H. Kamada, and A. Nogga, Few-Body Syst. **54**, 2427 (2013).

[6] I. Fachruddin, W. Glöckle, Ch. Elster, and A. Nogga, Phys. Rev. C **69**, 064002 (2004).

[7] K. Topolnicki, Ph.D. thesis, Jagiellonian University (unpublished).

[8] Wolfram Research, Inc., Mathematica, Version 11.3, Champaign, Illinois, 2018.

[9] W. Glöckle, *The Quantum Mechanical Few-Body Problem* (Springer-Verlag, Berlin, 1983).

[10] J. Golak, W. Glöckle, R. Skibiński, H. Witała, D. Rozpędzik, K. Topolnicki, I. Fachruddin, Ch. Elster, and A. Nogga, Phys. Rev. C **81**, 034006 (2010).

[11] M. Rodrguez-Gallardo, A. Deltuva, E. Cravo, R. Crespo, and A. C. Fonseca, Phys. Rev. C **78**, 034602 (2008).

[12] K. Topolnicki, Eur. Phys. J A **53**, 181 (2017).

[13] Y. Saad, *Numerical Methods for Large Eigenvalue Problems* (Manchester University Press, Manchester, 1992).

[14] http://www.fz-juelich.de/ias/jsc/EN/Expertise/Supercomputers/JURECA/UserInfo/BoosterOverview.html?nn=1803700